Technical University of Crete
School of Production Engineering and Management

DSMC simulations of rarefied hypersonic flows

A thesis submitted for the partial fulfillments

for obtaining the degree of

Master of Science

by

Angelos Klothakis

Supervisor: Dr. Ioannis K. Nikolos, Associate Professor

Chania, July 2015

Technical University of Crete
School of Production Engineering and Management

DSMC simulations of rarefied hypersonic flows

by

Angelos Klothakis

Approved by:

Dr. Ioannis K. Nikolos
Associate Professor
Technical University of Crete
School of Production Engineering
& Management

_____

Dr. Anargyros I. Delis
Associate Professor
Technical University of Crete
School of Production Engineering
& Management

_____

Dr. Efstratios Ioannidis
Assistant Professor
Technical University of Crete
School of Production Engineering
& Management

_____

Chania, July 2015

"Intentionally Left Blank"

Short CV

Angelos Klothakis was born in Chania in 1985, where he grew up and completed his basic education. In 2003 he was accepted in the School of Production Engineering and Management, Technical University of Crete. After he finished his studies he joined the army. After completing the army service he was accepted in the Postgraduate Program of the Technical University of Crete in the sector of Production Systems. With the completion of this thesis he completes the Postgraduate Program.

"In physics the truth is rarely perfectly clear, and that is certainly universally the case in human affairs. Hence, what is not surrounded by uncertainty cannot be the truth."

Richard P. Feynman

"Intentionally Left Blank"

Abstract

When the conditions of the flow are rarefied and hypersonic, a more suitable alternative to the use of Navier-Stokes equations for developing a numerical solution is the Direct Simulation Monte Carlo method (DSMC). The method was developed about 50 years ago by Graeme Bird [1] and now is a well-established technique for modelling low density gas flows. DSMC is a particle method, which employs a large number of particles in modelling a rarefied gas. In this thesis the application and performance of a new open-source DSMC computational kernel, called SPARTA (Stochastic PArallel Rarefied-gas Time-accurate Analyzer) (as described in [2]) is reported. Four cases are examined: a) a hypersonic flat plate simulation and comparison with DAC (DSMC Analysis Code) [3]; b) a Mach 20.2 flow over a 70-degree planetary probe; and c) a Mach 15.6 flow over a flared cylinder d) a hypersonic flow around a biconic. Those test cases were selected in order to investigate the ability of the SPARTA open-source code in reproducing the fine features of the complicated flow phenomena connected with shock-boundary and shock-shock interactions, and its computational efficiency in a parallel computation environment. Moreover, additional objectives of this assessment procedure were the establishment of a "best-practice" for the construction of the computational grids around the examined bodies, and the gain of know-how on the optimal use of the open-source code.

The aforementioned test cases, along with their variants, have been previously used by other researchers to validate some of the very well-known parallel DSMC solvers, such as DAC [3], SMILE [4], MONACO [5], ICARUS [6], MGDS [7] and dsmcFoam [8]. For example, dsmcFoam solver, among other test cases, was also validated against the flow over the 70-degree blunt cone [9]. DAC solver, which is NASA's code for DSMC simulations, has been validated against a 25/65 degrees sharp cone [10]. Furthermore, MONACO has been tested on a flow over a blunt cone, along with other validation cases, such as a blunt cone at an angle of attack [11]. Some important characteristics of the flows developed around the test objects are very steep gradients of velocity, temperature and density, shock/shock interaction, compression and rapid expansion. Such features render the numerical simulation of these complex flows very demanding so that a special study on the simulation parameters (number of particles, grid density, time step, etc.) is needed.

For the flat plate test case, simulation experiments have been conducted in a free-jet expansion tunnel [12], forming a database to be used for code validation purposes. Regarding the planetary probe test case, its form was decided by the AGARD Group 18 [13], while the experimental results, to be used for code validation, can be found in [13], [14]. Regarding the flared cylinder test case, a large number of experiments have been conducted in order to acquire accurate aero-thermodynamic results. The experiments were conducted on the SR3 wind tunnel, using nitrogen as the flow gas. The flared cylinder and the biconic experiments, used in this study, were conducted at the Buffalo Research Center (CUBRC) wind tunnel [15], [16]. These test cases were selected because the shapes used have the ability to reproduce shock/shock and shock/boundary interactions.

Περίληψη

Όταν η ροή είναι αραιή και οι συνθήκες της ταχύτητας υπερηχητικές, τότε η πιο ιδανική εναλλακτική μέθοδος επίλυσης της ροής αντί για τη χρήση των κλασσικών εξισώσεων Navier-Stokes είναι η Direct Simulation Monte Carlo (DSMC). Η μέδοθος αναπτύχθηκε πρίν από περίπου 50 χρόνια από τον Graeme Bird [1], και σήμερα είναι η πιο διαδεδομένη μέθοδος για την επίλυση τέτοιου είδους ροών. Η DSMC είναι μια μοριακή μέθοδος επίλυσης της ροής, όπου χρησιμοποιεί έναν μεγάλο αριθμό μορίων προκειμένου να μοντελοποιήσει το αραιό αέριο. Σε αυτή την εργασία εξετάζεται η εφαρμογή και η απόδοση ενός ανοικτού κώδικα DSMC kernel, που ονομάζεται SPARTA (Stochastic Parallel Rarefied-gas Time-accurate Analyzer) όπως αυτός περιγράφεται στη πηγή [2]. Τέσσερις test cases εξετάζονται στην παρούσα εργασία: α) Η υπερηχητική ροή γύρω από μια επίπεδη πλάκα, περιλαμβάνοντας τη σύγκριση των αποτελεσμάτων με τον κώδικα DAC (DSMC Analysis Code) της NASA [3]; β) Μια ροή με αριθμό Mach 20.2 γύρω από μια κάψουλα επανεισόδου στην ατμόσφαιρα ; γ) Ροή με αριθμό Mach 15.6 γύρω από έναν κεκλιμένο κύλινδρο; δ) Υπερηχητική ροή γύρω από έναν διπλό κόνο. Οι συγκεκριμένες test cases επιλέχθηκαν έτσι ώστε να μελετηθεί η ικανότητα του ανοιχτού κώδικα SPARTA στην προσομοίωση των δύσκολων φυσικών φαινομένων που συμβαίνουν σε τέτοιες ροές, όπως αλληλεπιδράσεις κυμάτων κρούσης μεταξύ τους και με τα όρια του υπολογιστικού χωρίου, καθώς και η απόδοση του κώδικα σε περιβάλλον παράλληλης επεξεργασίας. Επιπλέον, μελετήθηκαν και διάφορες πρακτικές κατασκευής υπολογιστικών πλεγμάτων, με σκοπό την βελτίωση των αποτελεσμάτων του κώδικα, και παράλληλα την απόκτηση εμπειρίας στη χρήση του.

Οι προς μελέτη test cases έχουν μελετηθεί και στο παρελθόν από διάφορους ερευνητές προκειμένου να πιστοποιηθούν, ως προς την ποιότητα των αποτελεσμάτων που παράγουν, ορισμένοι από τους πιο διαδεδομένους κώδικες DSMC παράλληλης επεξεργασίας, όπως οι DAC [3], SMILE [4], MONACO [5], ICARUS [6], MGDS [7], και dsmcFoam [8]. Ο κώδικας dsmcFoam στη συγκεκριμένη εργασία συγκρίνεται με τον SPARTA για την test case της ροής γύρω από μια κάψουλα επανεισόδου στην ατμόσφαιρα [9]. Στο παρελθόν ο DAC, ο οποίος είναι ο επίσημος DSMC κώδικας που χρησιμοποιείται από την NASA, πιστοποιήθηκε επιλύοντας τη ροή γύρω από ένα διπλό κώνο με 25 μοίρες κλίση για τον πρώτο και 65 μοίρες κλίση για τον δεύτερο κώνο [10]. Επίσης και ο MONACO έχει πιστοποιηθεί στα πρώτα στάδια της ανάπτυξης του επιλύωντας την ροή γύρω απο μία κάψουλα επανεισόδου στην ατμόσφαιρα με συγκεκριμένη γωνία προσβολής ως προς την ροή [11]. Κάποια σημαντικά χαρακτηριστικά των ροών που αναπτύσσονται γύρω από τα δοκίμια που χρησιμοποιούνται στις test cases είναι οι πολύ απότομες μεταβολές των μακροσκοπικών ποσοτήτων της ροής, τα αλληλεπιδρούμενα κύματα κρούσης και η συμπίεση και απότομη εκτόνωση των προς μελέτη αερίων. Τα χαρακτηριστικά αυτά, προκειμένου να αναλυθούν σωστά, απαιτούν μια ξεχωριστή μελέτη κάθε φορά ώστε να εντοπιστούν οι κατάλληλες παράμετροι (όπως χρονικό βήμα, αριθμός μορίων, πυκνότητα του πλέγματος κ.λπ.), ώστε να είναι δυνατή η ακριβής επίλυση, αυτού του είδους των ροών.

Για την test case της επίπεδης πλάκας αρχικά τα πειράματα έγιναν σε μια free-jet αεροσήραγγα [12], προκειμένου να συνταχθεί μια βάση δεδομένων, η οποία θα μπορούσε αργότερα να χρησιμοποιηθεί για την πιστοποίηση υπολογιστικών κωδίκων. Όσον αφορά στην test case με την κάψουλα επανεισόδου, τα προς μελέτη πειράματα σχεδιάστικαν από το AGARD Group 18 [13], ενώ τα πειραματικά δεδομένα που χρησιμοποιούνται για την πιστοποίηση κωδίκων μπορούν να βρεθούν στις πηγές [13], [14]. Για την test case του κεκλιμένου κυλίνδρου, έγινε ένας μεγάλος αριθμός πειραμάτων με διάφορες συνθήκες ροής, προκειμένου να εξαχθούν ακριβή θερμοδυναμικά αποτελέσματα. Τα περισσότερα πειράματα πραγματοποιήθηκαν στην αεροσήραγγα SR3, η οποία χρησιμοποιεί άζωτο ως εργαζόμενο μέσο. Στη συγκεκριμένη εργασία τα πειραματικά δεδομένα, που χρησιμοποιήθηκαν για τη σύγκριση με τα

υπολογιστικά δεδομένα, όσον αφορά στις test cases με τον κεκλιμένο κύλινδρο και τον διπλό κώνο έχουν παρθεί από τα πειράματα που έγιναν στην αεροσήραγγα του Buffalo Research Center (CUBRC) [15], [16]. Οι συγκεκριμένες test cases επιλέχθησαν διότι τα σχήματα των δοκιμίων που χρησιμοποιήθηκαν στα εν λόγω πειράματα έχουν την ικανότητα να δημιουργούν αλληλεπιδρούμενα κύματα κρούσης.

Acknowledgements

First of all, I would like to express my deepest gratitude to my supervisor Dr. Ioannis K. Nikolos, for giving me this wonderful opportunity to complete this thesis under his supervision, it is truly an honor. I would like to thank him for all the advice, ideas, moral support, and patience in guiding me through this thesis.

A special thanks also goes to my fellow labmates, PhD students George Strofylas, Sotirios Sarakinos, and Dr. George Lygidakis, for sharing their knowledge in the CFD field, CAD modeling and grid construction techniques. Besides that, I will also like to thank them for their friendship and for making my time in lab so enjoyable. A special thanks also goes to Dr. Michael A. Gallis and Steve J. Plimpton in Sandia National Laboratories for answering all my numerous emails and for their cooperation in resolving several bugs of the code.

Finally I would like to thank all my close friends, family, for their continuous love and support all these years. This thesis is dedicated to all of them.

Angelos Klothakis

"Intentionally Left Blank"

List of Tables

List of Figures

Table of Contents

"Intentionally Left Blank"

Introduction

Rarefied flow fields are very important as they are widely present in many and significant different topics, such as industrial and aerospace applications [17] and a lot of research is guided through this particular regime. At the beginning of the 20th century Knudsen Weber and other researchers, started to analyze the rarefied gas dynamics. Knudsen for example, studies the mass flow rate in a pipe, discovered the transitional regime and formulated the very well-known Knudsen number, which as we will see later, is a dimensionless number that characterize if a flow field is continuum or rarefied.

About 1960 there was a keen interest in space missions, so the rarefied regime was studied also in space applications due to the re-entry of space vehicles. At that altitude the flow is no longer continuum and special assumptions had to be made in order to analyze such flows. At about the same period Graeme Bird gave a fundamental contribution to rarefied analysis and invented the DSMC method [1], that in nowadays is the unique reliable method to examine rarefied flow fields. The paradox in these flow fields is that the Navier-Stokes are correct but cannot be used because the transport equations of Newton, Fourier and Fick fail. Besides that, the Boltzmann equation is valid but it is impossible to solve for a large number of particles.

Several studies made during the past years trying to reduce the computational cost of the Boltzmann equation [18], [19], but still the Boltzmann equation is very difficult to solve for large systems with different kind of particles. There was a need for a method that could simulate rarefied flows in a way so that it will not be dependent to the Boltzmann equation. Graeme Bird proposed the DSMC method which could accomplish that ambition by using a molecular description of the flow and by examining the flow in a more statistical and stochastic way. At its beginning as Bird mentions the DSMC method was not accepted by the scientific community, mostly because of its stochastic nature and because the results produced were accurate for simple flows. The following years the method was improved and performed better and several years later it was very widely accepted as the ultimate method for analyzing rarefied flows.

The need for simulation of larger systems and in many different flight conditions has been evolved in the 90's. The DSMC method is very computationally intensive in elevated pressures and for large systems. This problem was the cause for the beginning of developing parallel DSMC codes. The first parallel DSMC code developed was DAC by G.J. LeBeau [3] which also is NASA's production DSMC code. Also many other codes exist such as SMILE [4], MONACO [5], ICARUS [6], MGDS [7], dsmcFoam [8] and the most recent one SPARTA [2]. Most of these codes have been used in very intense and difficult simulations and have proven their value over the years. In this thesis the parallel DSMC kernel SPARTA was used in the simulation of all cases in order to verify the efficiency and the quality of the results the code produces for hypersonic rarefied flows. Five different test cases used in literature for code validation purposes are examined in order to compare the computed and the experimental results. Moreover the results are also compared with the results obtained from other codes such as dsmcFoam, DAC, MONACO and DS2V.

SPARTA is a very flexible DSMC code which can be modified in order to try new approaches or used as is. Although its flexibility it is not for the amateur user. It is a requirement to have a knowledge in the DSMC method and rarefied gases as it needs to define a lot of parameters in order to perform a simulation accurately. The most important of them is the number density, timestep, and the multilevel Cartesian grid as it will be described later. In order to perform a simulation with SPARTA one must write an input script.

The input script is written in such a way the code can understand and setup the parameter required for the simulation. A typical input script has four parts:

1. Initialization
2. Problem definition
3. Simulation settings
4. Run simulation

Each part of the input script will be defined analytically later. SPARTA can run in 2d 2d-axisymmetric and 3d domains and has a variety of boundary conditions. Furthermore there are a variety of different molecular models as well such as VSS (Variable soft sphere), VHS (Variable hard sphere), HS (Hard sphere) and in the latest version two chemistry models have been implemented, TCE and the Q-K (Quantum Kinetic) models. Moreover SPARTA is a core DSMC code, it not accompanied by any GUI or pre-processor which adds complexity for the amateur user. Besides that, as it will be shown in later chapters if used wisely the code produces very accurate results for very complex flows.

In this thesis SPARTA is put into a test and used in order to simulate some of the most demanding code validation experiments in order to validate the code results and performance. As it will be noted in later chapters there is an excellent agreement between computed and experimental results as well as there is also a good agreement in results calculated with other well-known DSMC codes. Moreover SPARTA performance is also tested and the codes features such as the gridcuts and the dynamic-balancing which offer some speedup performance. Finally we have to mention that the code is being updated from quite often and there are always some new features added or bugs corrected.

The first case we examine is a flat plate simulation in rarefied gas with hypersonic speed. We measure the pressure on the upper surface of the plate and the heat transfer on that surface. Next the geometry of Mars Pathfinder probe was designed and from experimental data obtained from literature the experiment of the Mars Pathfinder reentry was performed. In this test case we can evidence very interesting flow effects. This case has been simulated with 2 different gases a rarefied and a denser one. On the denser simulation the vortexes at the back of the cone can be seen more clearly due to the higher density of the flow. For this case the heat transfer on the blunt cone surface is measured. The next two cases are trickier than the previous ones as there are shock-boundary and shock-shock interactions. On the flared cylinder case and on the biconic case except from the heat transfer on the surface also the pressure on the surface is taken into account. As far as the flared cylinder is concerned the results are compared not only with the experimental but also with results obtained for DS2V a well-established DSMC code written by Graeme Bird.

For every case simulated there are also Figures which so the axisymmetric surface rotated by its axis of symmetry so that the real 3d surface can be obtained. On the 3d surface we can see the heat transfer from the flow to the surface as well as the pressure and the shear stresses. This is done in order to get a better understanding of the flow interaction on the surface.

The outline of this thesis is:

➢ Chapter 1. A brief overview of the DSMC theory is given along with different molecular models simulation parameters and sampling methods.
➢ Chapter 2. Description of the SPARTA DSMC kernel and how to define a problem.
➢ Chapter 3. Description of all the test cases simulated by the code and comparison of the computed and experimental results.

➢ Chapter 4. Conclusion remarks and future work.

The DSMC Method

1.1 Introduction

The DSMC method was first introduced by Graeme Bird in the early 1970s [1] is a particle-based model, which studies the rarefied flow in a direct physical way instead of solving any equations. In other words, the evolution of a large number of simulated particles, which represent a fraction of the real molecules in the flow field, is simulated. Modeling is implemented by uncoupling the particle's motion and calculating the intermolecular collisions between the simulated particles over a small time interval. In general the DSMC method consists of four steps:

1. Moving of particles
2. Indexing particles into cells
3. Performing the intermolecular collisions
4. Sampling particles properties

In order to locate the particles and track their movements, the whole computational domain is divided into a number of cells, which contain sub-cells in a predefined structure. Initially, a set of particles are randomly distributed in each cell. Each of the particles is assigned a position, velocity components and energy. Then, the mentioned steps are repeated in each time step in order to simulate the evolution of flow in time. The macroscopic quantities of the flow, such as velocity, pressure, density, temperature and so on, are measured on each cell and can be obtained from simple weighting averages of microscopic properties.

1.1.1 Discretization in time and space

The essential approximation made in DSMC simulations is that over a small time interval or step Δt the molecular motion is independent of the intermolecular collisions. Accordingly, each molecule is moved by its corresponding distance traveled in this time interval, taking interactions with flow boundaries into account. After the calculation of the molecular moves the time is advanced by one time step and an appropriate set of intermolecular collisions is selected. By alternating moving and colliding the flow develops from its initial state with time in a physically realistic manner. Usually a uniform flow is chosen as the initial state of the gas, which is specified by means of the macroscopic stream velocity, and two state variables such as number density and temperature. Accordingly, neither an initial estimate of the flow field nor any kind of iteration is needed. All simulations are unsteady in the sense that they employ a time parameter which may be identified with physical time in real flow. However, if the boundary conditions allow the formation of a steady flow, the steady state may be attained as an average of the unsteady flow over time. The uncoupling of the molecular motion and intermolecular collisions is valid as long as the time step is small compared to the local mean collision time and if this condition is met the results are independent of its actual value [1].

The grid in physical space serves the purpose of selecting the appropriate collision partners within each grid cell and afterwards sample the macroscopic flow properties. The more molecules used in a simulation the finer is the grid and the shorter gets the separation distance between colliding particles. This leads to a more accurate representation of the real flow behavior and thus improves the quality of the results. The computation time of the DSMC routines is generally proportional to the number of simulated molecules, this is at the cost of higher computational efforts. This tradeoff gains importance at low Knudsen numbers and shorter mean free paths such as in the continuum regime. Bird in 2005 [17] proposed the ration of mean collision separation (MCS) to the mean free path (MFP) as the most important quality criterion for DSMC simulations and recommended an upper limit of

$$\frac{MCS}{MFP} < 0.2 \hspace{4cm} 1.1$$

as higher values could cause distortions of the results. Advantage may be taken of flow symmetries in order to reduce the computation effort. The cell grid is simply required in the spatial directions with varying flow properties and the mean collision separation is measured in these dimensions only. Consequently the number of molecules needed and also the number of position coordinates that have to be stored can be reduced in such a simulation, while the flow domain itself and the collisions are still three-dimensional [1].

1.1.2 Applicability of the method

In the classic kinetic theory of gases the dominant equation which simulates the collisions between the molecules of a gas is the Boltzmann equation. However, Boltzmann's equation is extremely computationally intensive. Through the years a variety of approximation models have been proposed in order to simplify the equation but the solution of the equation was still very hard. The main reason for the invention of the DSMC method was the need for a method that could simulate the behavior of rarefied gases but by bypassing the solution of the Boltzmann equation. The procedures for the probabilistic choice of appropriate collisions though, are still based on relations from the classical kinetic theory of gases. Therefore the DSMC method is subject to the same limitations as the Boltzmann equation. The principal requirements for the applicability of the method are a dilute gas and molecular chaos. The general definition of a dilute gas is given by

$$\delta \gg d \hspace{4cm} 1.2$$

where $\delta = n^{-1/3}$ is the mean molecular spacing and d the diameter of the molecules. In such a gas the fraction of volume that is occupied by the gas molecules is very small and the motion of each molecule is unaffected by other molecules for the most part. In addition, if there is a collision between molecules, it is overwhelmingly probable that only two molecules are involved, so binary collisions need to be considered only. The assumption of molecular chaos basically requires that the molecules move independently of each other and therefore the probability of finding two molecules in a certain two particle configuration is simply the product of probabilities of finding each molecule in each corresponding

one particle configuration. Consequently the DSMC method cannot be used to simulate dense gases or plasmas with a high portion of ionized particles that are affected by long-range interactions. In addition DSMC utilizes models of gas molecules and boundary interactions developed in kinetic theory, which provide only an approximation to real physics. An important difference to the Boltzmann equation is that DSMC does not rely on inverse collisions. Furthermore the boundary conditions in direct simulations are defined by the behavior of individual molecules rather than by means of a distribution function. This enables the incorporation of complex flow phenomena such as chemical reactions, which cannot be considered in the analytical model [1].

1.1.3 Sampling of macroscopic properties

The DSMC method provides information on the position, velocity and state of every molecule at all times, which enables the sampling of macroscopic flow properties such as density, pressure and temperature at any location in the flow. Accordingly, the simulation results can be expressed in terms of quantities that are well known from continuum analyses. The relations between microscopic and macroscopic quantities may be found in any book on kinetic theory. In this section some general issues related to the calculation of macroscopic properties are concerned and two averaging techniques are discussed.

Macroscopic quantities are associated with a spatial location in the flow and have to be based on the state of the molecules in a cell enclosing this particular point. In a volume cell V with number density n there are N_r real molecules and this number follows a Poisson distribution about the mean value nV with standard deviation $\sqrt{nV}$,

$$P(N_r) = \frac{(nV)^{N_r}}{N_r!} e^{-(nV)} \qquad 1.3$$

A normalized measure of dispersion in statistics is the coefficient of variation, which is defined as the ratio of the standard deviation to the mean value,

$$CV(N_r) = \frac{\sqrt{Var(N_r)}}{E(N_r)} = \frac{1}{\sqrt{nV}} \qquad 1.4$$

The number of simulated molecules within the same volume V is denoted by N and is Poisson distributed with mean value and variance equal to nV/F_N

$$P(N) = \frac{(nV/F_N)^N}{N!} e^{-(nV/F_N)} \qquad 1.5$$

where F_N is the number of real molecules represented by each simulation molecule. Its variation coefficient is given by

$$CV(N) = \sqrt{\frac{F_N}{nV}} \qquad\qquad 1.6$$

From equations (1.4) and (1.6) it is seen that the statistical fluctuations in real gases are amplified by the factor $\sqrt{F_N}$ in DSMC simulations, and as F_N can easily be in the range of 10^{10} to 10^{12}, this effect is significant. Using the definition of the mean molecular spacing nV can be written as V/δ^3. Consequently, in order to limit the level of scatter to a reasonable level, the linear dimensions of the cell, over which the instantaneous macroscopic properties are sampled, should satisfy the condition

$$V^{1/3} \gg F_N^{1/3}\delta \qquad\qquad 1.7$$

In addition the linear dimensions of the cells in every direction should be small compared to the local scale length of the macroscopic gradients in the gas in that particular direction, in order to ensure a good resolution of the flow. In practical applications of the DSMC method this is usually not possible without violating the scattering condition stated above. However, equation (1.7) needs to be met only for instantaneous averages and can thus be mitigated by alternative averaging techniques.

The first one is called time average and is established by summing the properties of the molecules in the cells over a certain time interval. This enables any steady flow to be described in terms of macroscopic quantities. The second average is built from the instantaneous averages over the molecules in the corresponding cell in a large number of similar systems. By means of this so-called ensemble average the macroscopic quantities of an unsteady flow may be established by repeating the experiment multiple times. Time and ensemble averages can be used to establish macroscopic quantities of practically every flow. Unfortunately both techniques are stochastic and thus subject to fluctuations. The standard deviation is inversely proportional to the square root of the sample size and may thus be reduced to any desired level by increasing the sampling interval for time averaging or the number of repetitions for ensemble averaging respectively. The accomplishment of a certain accuracy of the results is sometimes referred to as convergence, which is not to be confused with the convergence of conventional CFD procedures from an initial approximation to the exact solution [1].

1.1.4 Collisions sampling

The proper choice of collision pairs and the realization of the correct number of collisions, is crucial to the consistency of the simulation with the physical flow processes. In order to model the collisions accurately we consider a cell of volume V_c and number density n. This cell contains nV_c real molecules and the average number of simulated molecules is given by $\bar{N} = nV_c/F_N$. The actual number of simulated molecules is denoted by N, which is a stochastic variable. According to kinetic theory the total number of collisions N_T in a time step Δt within this cell is calculated by the equation

$$N_T = \frac{1}{2}Nv\Delta t = \frac{1}{2}Nn\overline{\sigma_T c_r}\Delta t \qquad\qquad 1.8$$

where $v = n\overline{\sigma_T c_r}$.

Various procedures for the random sampling of collisions within a cell have been developed over the years but here only the most efficient and widely used technique is described, namely the no time counter method (NTC) proposed by G.A Bird [1] and validated by M.A. Gallis et al [18].

In NTC the probability of a collision to occur between two molecules in a time interval Δt can be calculated as the ratio of the volume swept out by their total cross section $F_N \sigma_T$ at relative speed c_r to the cell volume,

$$P = \frac{F_N \sigma_T c_r \Delta t}{V_c} \tag{1.9}$$

One sampling probability is to compute for all $N(N-1)/2$ potential collision pairs and to select each collision with its corresponding probability of occurrence. However, the efficiency of this so-called direct method is low, because P is usually very small and the computation time is proportional to the square of the number of molecules in the cell. Therefore the NTC method considers only a fraction of all possible collision pairs and their probability is increased by dividing equation (1.9) by this fraction. In order to achieve maximum efficiency the fraction is chosen such that the maximum that the maximum probability equals to unity. The fraction is given by

$$P_{max} = \frac{F_N (\sigma_T c_r) \Delta t}{V_c} \tag{1.10}$$

Initially the maximum product of collision cross-section and relative speed $(\sigma_T c_r)_{max}$ can be chosen sufficiently large and then is altered as higher values during the simulation. The number of collision pairs considered per time step is obtained by multiplication of (1.10) by $N(N-1)/2$. However, as N is subject to statistical fluctuations it is recommended to replace $N(N-1)$ by the product of instantaneous value and a time or ensemble averaged value $N\overline{N}$. In relation to that the number of molecule pairs considered for collision per time step in the NTC method is equal to

$$\frac{1}{2} \frac{N\overline{N} F_N (\sigma_T c_r)_{max} \Delta t}{V_c} \tag{1.11}$$

and the collision is selected with probability

$$P = \frac{\sigma_T c_r}{(\sigma_T c_r)_{max}} \tag{1.12}$$

The number of collisions that are realized per time step is not affected by the exact value of P_{max} and amounts to

$$N_{T,NTC} = \frac{1}{2} \frac{N\bar{N}F_N \overline{\sigma_T c_r \Delta t}}{V_c} = \frac{1}{2} Nn\overline{\sigma_T c_r \Delta t} \qquad 1.13$$

This number is in agreement with the theoretical value obtained by the equation (1.8) and it is observed that this procedure yields a computation time that is linear in N [1].

1.2 The need for a molecular description

The degree of rarefaction of a gas is expressed through the Knudsen number which is the ratio of the mean free path λ to the characteristic dimension L,

$$Kn = \frac{\lambda}{L} \qquad 1.14$$

It is more precise to specify a local Knudsen number by defining L as the scale of the local macroscopic gradients,

$$L = \frac{\rho}{\partial p / \partial x} \qquad 1.15$$

When the Knudsen number is small compared to unity, the scale of macroscopic gradients is big compared to the local mean free path, then the transport terms in the Navier-Stokes equations can be defined properly and are valid. On the contrary, it is traditionally admitted that the Navier-Stokes should not be used when the Knudsen number is bigger than 0.1.

1.3 Binary elastic collisions

In order to simulate the molecular movement, a physical model of collisions between molecules is necessary. In dilute gases, which are the major application of the DSMC method, the probability of a collision including more than two particles is so small that only binary collisions are considered. The term elastic collision means that collisions are performed without interchange of energy between translational and internal modes.

1.3.1 Momentum and energy considerations

Let's consider a collision between two molecules with pre-collision velocities c_1 and c_2 and masses m_1 and m_2. Our objective is to determine their post-collision velocities c_1^* and c_2^*. Let $c_r = c_1 - c_2$ be the relative velocity between the two particles and c_m the velocity of their center of mass. Conservation of linear momentum and energy in the collision lead to equation in [1]:

$$c_1^* = c_m + \frac{m_2}{m_1 + m_2} c_r^* \qquad\qquad 1.16$$

$$c_2^* = c_m - \frac{m_2}{m_1 + m_2} c_r^* \qquad\qquad 1.17$$

As the magnitude of the relative velocity remains unchanged and the movement of the center of mass is not affected by the collision, the determination of the post-collision velocities reduces to the calculation of the change in direction x of the relative velocity vector. The reduced mass m_r is defined by:

$$m_r = \frac{m_1 * m_2}{m_1 + m_2} \qquad\qquad 1.18$$

Intermolecular collisions are often created by strong interactions between the force fields of the molecules. These force fields are traditionally assumed to be spherically symmetric and have typical attraction-rejection form. That means that the force is zero at large distances, weakly attractive in small distances and strong at very short distances. Then the dynamics of the collision are given by the classical two-body problem and summarized in figure 1.1 [1]. It can be shown that the motion of the molecule of mass m_1 relative to the molecule of mass m_2 is equivalent to the motion of a molecule of mass m_r relative to a fixed center of force.

1.3.2 Impact parameters and collision cross-sections

Apart from the velocities of the two molecules, just two other impact parameters are required to completely specify a binary elastic collision. The first is the distance of the closest approach b of the undisturbed trajectories in the center of mass frame of reference and the second is the angle e between the collision plane (the pre-collision and post-collision trajectories of the molecules must rely on the same plane) and a reference plane, as shown in figure 1.2 [1].

The parameters b and e give a certain deflection angle x. The differential cross-section $\sigma d\Omega$ corresponding to the parameters b and e is defined by

$$\sigma d\Omega = bd\ bde \qquad\qquad 1.19$$

where $d\Omega$ is the unit solid angle about the vector c_r^*. From figure 1.2 we can see that

$$d\Omega = \sin x\, dx\, de \qquad\qquad 1.20$$
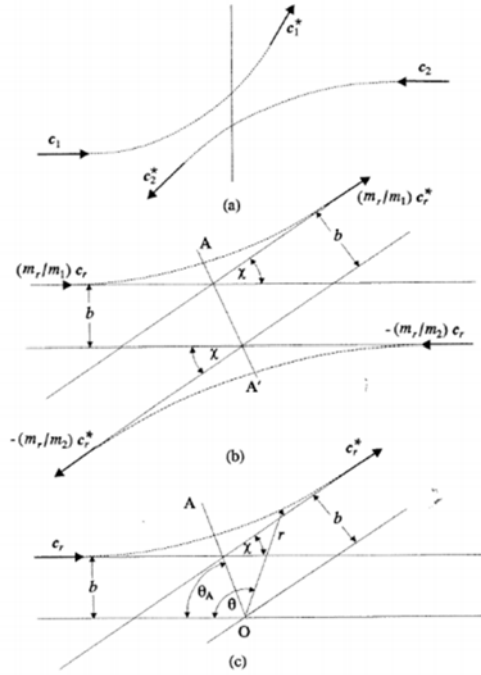
Figure 1.1 Representations of the binary collision: a) Laboratory frame of reference b) Binary collision in the center of mass frame of reference c) Interaction of reduced mass particle with a fixed scattering center

so that

$$\sigma = \frac{b}{|\sin x|}\frac{db}{dx} \qquad\qquad 1.21$$

The total collision cross-section σ_T is defined by

$$\sigma_T = \int_0^{4\pi} \sigma d\Omega = 2\pi \int_0^{\pi} \sigma \sin x\, dx \qquad\qquad 1.22$$

The viscosity cross-section σ_μ is defined by

$$\sigma_\mu = \int_0^{4\pi} (\sin^2 x)\, \sigma d\Omega = 2\pi \int_0^{\pi} \sigma(\sin^3 x)dx \qquad\qquad 1.23$$
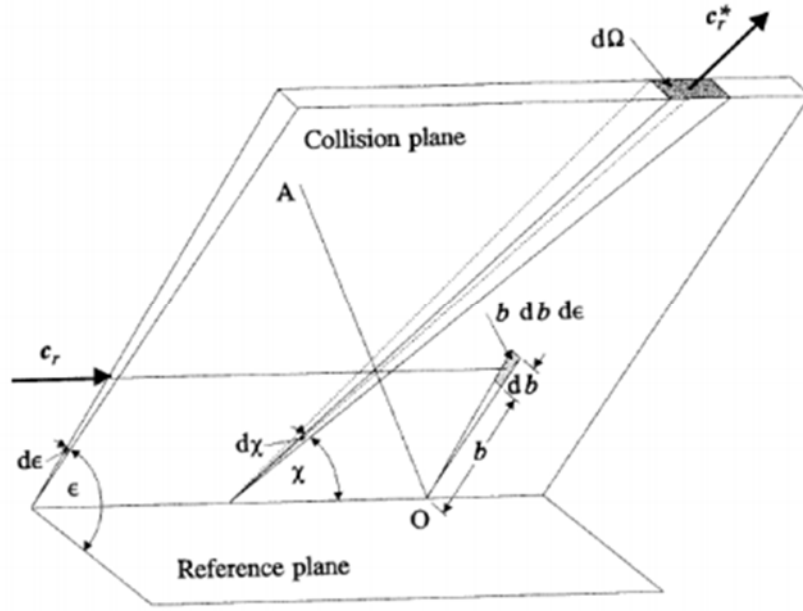
Figure 1.2 Impact parameters

The component of the post-collision velocity perpendicular to the direction of the pre-collision velocity is $c_r \sin x$. This integral is used in the Chapman-Enskog theory [1], in order to calculate the coefficient of viscosity.

The momentum transfer cross-section also called the diffusion cross-section is defined by

$$\sigma_M = \int_0^{4\pi} (1 - \cos x)\, \sigma d\Omega = 2\pi \int_0^{\pi} (1 - \cos x) \sin x \, dx \qquad 1.24$$

The component of the post-collision velocity perpendicular to the direction of the pre-collision velocity is $c_r(1 - \cos x)$, and this integral is also used in the Chapman-Enskog theory in order to calculate the diffusion coefficients.

1.3.3 Determination of the deflection angle x

In the third frame shown in figure 1.1 the equation for the angular momentum is

$$r^2\theta = cst = bc_r \qquad 1.25$$

The energy of a molecule is the sum of its kinetic energy and its potential energy φ and it must be equal to the energy at infinity, where potential energy vanished, so

12

$$\frac{1}{2}m_r(\dot{r}^2 + r^2\dot{\theta}^2) + \varphi = cst = \frac{1}{2}m_r c_r^2 \tag{1.26}$$

The potential energy φ is given by

$$\varphi = \int_r^\infty F dr \tag{1.27}$$

or

$$F = -d\varphi/dr$$

Solving these equations gives

$$\theta_A = \int_0^{W_1} [1 - W^2 - \varphi/(\frac{1}{2}m_r c_r^2)]^{-1/2} dW \tag{1.28}$$

where W_1 is the positive root of the equation

$$1 - W^2 - \varphi/\left(\frac{1}{2}m_r c_r^2\right) = 0 \tag{1.29}$$

and $W = \frac{b}{r}$ is a dimensionless coordinate. Finally, it can be seen from figure 1.1 that

$$x = \pi - 2\theta_A \tag{1.30}$$

To simplify it these equations mean that, once the force or potential are known, the specifications of the impact parameter b allows us to calculate the deflection angle and this is the last element needed in order to calculate the post-collision velocities. Let u_r , v_r , w_r be the pre-collision relative velocity Cartesian coordinates. Then the three components u_r^* , v_r^* and w_r^* of the post-collision relative velocity are given in the same Cartesian frame by the equation 1.22 [1]:

$$u_r^* = \cos x\, u_r + \sin e(v_r^2 + w_r^2)^{1/2},$$
$$v_r^* = \cos x\, u_r + \sin x\, \frac{c_r w_r \cos e - u_r v_r \sin e}{(v_r^2 + w_r^2)^{\frac{1}{2}}}, \tag{1.31}$$
$$w_r^* = \cos x\, w_r - \sin x\, (c_r v_r \cos e + u_r w_r \sin e)/(u_r^2 + w_r^2)^{1/2}$$

A molecular model must be specified to close the equations because the potential energy needed is in equation 1.15. This is the last step before being able to compute intermolecular collisions. The molecular

model is also necessary to calculate the total cross-section, which is needed in order to calculate the collision frequency. The collision frequency is a key parameter to define the time step of the simulation. A model always involves some degree of approximation and the goal here is to use a model that leads to sufficient agreement between theory and experiment. Here will be presented only four models that are commonly used in DSMC. These are the inverse power law model, the hard sphere model (HS), the variable hard sphere model (VHS) and the variable soft sphere model (VSS).

1.3.4 The inverse power law model

This model is defined by

$$F = \kappa/r^{\eta},$$
$$\varphi = \kappa/[(\eta - 1)r^{\eta-1}]$$

1.32

where κ and η are two constant parameters.

From this expression the deflection angle can be calculated. One important practical disadvantage of this model is that for a finite η the force field extends to infinity and the integral in equation 1.9 for the total cross-section diverges. This means that two molecules are always having a collision of some kind of interaction. However, most of these interactions involve extremely slight deflections because the molecules are far from each other. In practice, a finite cut-off on the force field is used so a finite cross-section can be calculated. But as this cut-off is arbitrary, the resulting total cross-section is not suitable for setting the effective collision frequency or mean free path. The inverse power law model is the most realistic model from the analytical point of view. It is therefore useful for analytical studies. However, it is not a suitable model for direct simulation collisions.

1.3.5 The hard sphere model

This is an over-simplified but useful model. The molecules are modeled as hard spheres and they collide, as shown in figure 1.3, when their distance decreases to

$$r = \frac{1}{2}(d_1 + d_2) = d_{12}$$

1.33

where d_1 and d_2 are the diameters of the colliding molecules. Its main advantages are a finite cross-section defined by

$$\sigma_T = \pi d_{12}^2$$

1.34

and an easy calculation of the collision. The scattering from hard sphere molecules is isotropic in the center of mass frame of reference. In other words, all directions are equally likely for c_r^*. In the hard sphere model the viscosity cross-section and diffusion cross-section defined by the equations 1.10 and 1.11, are respectively

$$\sigma_\mu = \frac{2}{3}\sigma_T$$

1.35

and

$$\sigma_M = \sigma_T$$

1.36
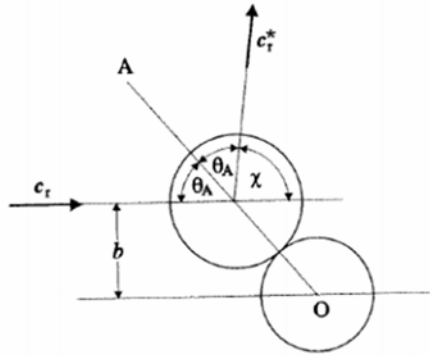
Figure 1.3: Collision geometry of hard sphere model

1.3.6 The variable hard sphere model (VHS)

The advantages of the hard sphere model are a finite cross-section and an isotropic scattering in the center of mass frame of reference. Unfortunately this scattering law is unrealistic. But the main drawback of the hard sphere model is its viscosity coefficient. According to Bird, molecular model for rarefied gas flows should reproduce the viscosity coefficient of the real gas and also the temperature dependence of this coefficient [1]. The viscosity of the hard sphere model is proportional to the temperature to the power of 0.5, whereas real gases have powers of the order of 0.75. The main reason for this lack of accuracy is that the total cross-section, as equation 1.21 shows, is independent of the relative translational energy $E_t = \frac{1}{2}m_r c_r^2$. The real cross-section depends on this relative velocity. Because of inertia, the change in the trajectories decreases when the relative velocity increases, so the cross-section must decrease when c_r increases. A variable cross-section is required to match the powers of order of 0.75 that are characteristic of real gases. This led to the variable hard sphere model (VHS).

The molecule is modeled as a hard sphere with a diameter d that is a function of c_r, more precisely an inverse power law,

$$d = d_{ref}\left(\frac{c_{r,ref}}{c_r}\right)^{\xi}$$ 1.37

where the subscript ref denotes reference values. The d_{ref} corresponds to the effective diameter at relative speed $c_{r,ref}$ and ξ is the VHS parameter. For a particular gas, the reference values are defined by the effective diameter at a particular reference temperature. The VHS model combines a finite cross-section that eases the calculation of collisions with a realistic temperature exponent of the coefficient viscosity. The deflection angle is given by

$$\chi = 2cos^{-1}\left(\frac{b}{d}\right)$$ 1.38

Both the inverse power law and the VHS model lead to a law temperature dependence of the coefficient of viscosity [1] such that

$$\mu \propto T^{\omega}$$ 1.39

where

$$\omega = \frac{1}{2} + \xi$$ 1.40

in the VHS model.

The coefficient ω of a real gas is determined experimentally and used to calculate the exponents η and v such that the inverse power law and the VHS models match the real temperature dependency of the viscosity. Finally, for a gas such that $\mu \propto T^{\omega}$ and with the reference viscosity μ_{ref} at the reference temperature T_{ref}, the VHS model is given by equation 3.68 in reference [1],

$$d = \sqrt{\frac{15}{8}\frac{\sqrt{\frac{m}{\pi}}(kT_{ref})^{\xi+1/2}}{\Gamma(4-\xi)\mu_{ref}E_t{}^{\xi}}}$$ 1.41

It is recommended to use this diameter to set the total collision cross-section of VHS molecules [1]

The coefficient of viscosity in the VHS molecular model is derived from the Chapman-Enskog theory and is equivalent to

$$\mu = \frac{15}{8} \frac{\sqrt{\pi m k} \left(\frac{4k}{m}\right)^{\xi} T^{\frac{1}{2}+\xi}}{\Gamma(4-\xi)\sigma_{T,ref} c_{r,ref}^{2\xi}} \qquad 1.42$$

In a gas composed of species 1 and 2 the diameter is calculated separately for each molecule and the effective diameter of the collision cross section is obtained from equation 1.20. However it is more appropriate to determine the total cross section of collisions between different molecules by means of the diffusion coefficient D_{12},

$$D_{12} = \frac{3}{8} \frac{\sqrt{\pi} \left(\frac{2kT}{m_r}\right)^{\frac{1}{2}+\xi_{12}}}{\Gamma(3-\xi_{12}) n\sigma_{T,ref,12} c_{r,ref}^{2\xi_{12}}} \qquad 1.43$$

The parameter ξ_{12} can be determined by the equation 1.27, if values are available for the exponent ω_{12} of the mixture, or alternatively set as the mean of the individual parameters. For a binary gas mixture with diffusion coefficient $D_{12,ref}$ at reference temperature T_{ref} the cross-collisional diameter is specified as a function of the relative translational energy such as,

$$d_{12} = \sqrt{\frac{3}{8} \frac{(2kT)^{\frac{1}{2}+\xi_{12}}}{\Gamma(3-\xi_{12})\sqrt{\pi m_r n D_{12,ref}}(2E_t)^{\xi_{12}}}} \qquad 1.44$$

In general a difference between the mean of the viscosity based diameters and the cross-collision diameter defined by the diffusion coefficient, the ability of the VHS model to reproduce the correct transport properties in a gas mixture might be limited [1].

1.3.7 The Variable Soft Sphere Model (VSS)

The most recent popular molecular model used in DSMC simulations is the Variable Soft Sphere model (VSS) developed by Koura and Matsumoto [19]. In this model the dependence of the variable soft sphere diameter with relative speed is equivalent to the equation 1.24, the deflection angle is modified to

$$\chi = 2\cos^{-1}\left(\left(\frac{b}{d}\right)^{1/a}\right) \qquad 1.45$$

Here a is the VSS scattering parameter. The total collision cross section of a variable soft sphere is given by $\sigma_T = \pi d^2$. As a result this leads to the viscosity expression of a VSS gas,

$$\mu = \frac{5}{16} \frac{(\alpha+1)(\alpha+2)\sqrt{\pi m k}\left(\frac{4k}{m}\right)^{\xi} T^{\frac{1}{2}+\xi}}{\alpha\Gamma(4-\xi)\sigma_{T,ref}c_{r,ref}^{2\xi}}$$

1.46

Such as in the VHS model the viscosity here is also proportional to $T^{\frac{1}{2}+\xi}$ and the parameter ξ is chosen as in the VHS model. Similarly the diffusion coefficient in a VSS gas mixture is given by

$$D_{12} = \frac{3}{16} \frac{(a_{12}+1)\sqrt{\pi}\left(\frac{2kT}{m_r}\right)^{\frac{1}{2}+\xi_{12}}}{\Gamma(3-\xi_{12})n\sigma_{T,ref,12}c_{r,ref}^{2\xi_{12}}}$$

1.47

For a simple gas with viscosity μ_{ref} and self-diffusion coefficient $D_{11,ref}$ at the reference temperature T_{ref} the effective diameters d and d_{11} based on the viscosity and diffusion are given by

$$d = \sqrt{\frac{5}{16}\frac{(a+1)(a+2)\sqrt{m/\pi}\left(kT_{ref}\right)^{\xi+1/2}}{a\Gamma(4-\xi)\mu_{ref}E_t^{\xi}}}$$

1.48

and

$$d_{11} = \sqrt{\frac{3}{8}\frac{(a+1)\left(kT_{ref}\right)^{\xi+1/2}}{\Gamma(3-\xi)\sqrt{\pi m}D_{11,ref}E_t^{\xi}}}$$

1.49

respectively. By requiring equity for the two diameters a may be determined by

$$a = \frac{10\rho D_{11,ref}}{6(3-\xi)\mu_{ref} - 5\rho D_{11,ref}}$$

1.50

Consequently the VSS model reflects diffusion processes in gas mixtures more precisely than the VHS model and is thus more favorable for the analysis of diffusion phenomena. A limitation of the model is that constant values for a are generally only valid in a certain temperature range. Typical values for the VSS scattering parameter a of various gases at $0^o C$ are given in Ref. [1].

It has to be noted that the VHS and VSS models both approximate the realistic inverse power law model, i.e. they neglect the attractive potential at large intermolecular distances and show a finite total collision cross-section. In addition there are three popular models in the kinetic theory that include the attractive component, these are the Lennard-Jones potential [20], and similarly the generalized hard sphere (GHS) [21]and the generalized soft sphere (GSS) [22] models were developed to consider this effect in DSMC simulations.

1.4 Inelastic collisions and rotational relaxation

Except from the three translational velocity components diatomic and polyatomic molecules have rotational and vibrational degrees of freedom, which are also called internal modes. When two molecules are involved in an inelastic collision, energy is also exchanged between the different modes. This section will explain how this is implemented in the DSMC procedures.

1.4.1 Internal degrees of freedom

The characteristic temperatures of rotation Θ_r and vibration Θ_v indicate the point at which the corresponding degrees of freedom are excited. Typical values for the most common molecules used in DSMC are summarized in [1]. Usually, at ambient temperature (about 300K) the rotational degrees of freedom may be assumed to be fully excited whereas the vibrational modes are inactive. In the test cases examined at a later chapter only rotational modes are considered since the temperatures are not so high in order to encounter vibrational excitation.

Energy can only be stored in the rotation about an axis with high moment of inertia. This explains why diatomic molecules have two rotational degrees of freedom and there is no rotation about the intermolecular axis. As in the elastic collisions, phenomenological models are used in DSMC routines to simulate the energy exchange between rotational and translational modes, as the classical polyatomic models from kinetic theory of gases, such as the two centers of repulsion model, are impractical if millions of collisions have to be calculated. The most widely used model is that of Larsen and Borgnakke, which is described below [1].

1.4.2 The Larsen-Borgnakke model

The Larsen-Borgnakke model reallocates the total energy in an inelastic collision between the translational and internal degrees of freedom by sampling from the equilibrium distributions of these modes corresponding to the total energy. The appropriate relaxation time, such as the time required by a molecule to accomplish equilibrium between translational and internal energies, is established by regarding only a fraction Λ of collisions as inelastic. The other collisions are treated as completely elastic and are calculated according to the underlying atomic model. This approach has proved to reproduce a realistic relaxation behavior as described in detail in Ref. [1].

1.4.3 Rotational relaxation

A gas with collision rate ν is considered in which the rotational temperature T_r of a particular molecule differs from the overall temperature. Applying the Larsen-Borgnakke method to a fraction Λ of the collisions leads to a relaxation process characterized by

$$\frac{dT_r}{dt} = \nu\Lambda(T_e - T_r) \tag{1.51}$$

where T_e is the final equilibrium temperature in the gas. Integration of the above equation yields

$$T_r = T_e - (T_e - T_{r,0})e^{-\nu\Lambda t} \tag{1.52}$$

where $T_{r,0}$ is the initial rotational temperature at zero time and both ν and Λ are generally a function of temperature. The time in which the disturbance from equilibrium decreases by a factor of $1/e$ is defined as the relaxation time τ, and from Bird's book [1] we get

$$\tau = \frac{1}{\nu\Lambda} \tag{1.53}$$

The difficulty in DSMC simulations consists of determining the value of Λ for the fraction of inelastic collisions such as the correct relaxation rate is achieved. Some data exists in literature about the calculation of the rotational relaxation collision number Z_r, which may be regarded as the average number of collisions required to establish equilibrium. An approximate relation between Z_r and Λ is given by the simple formula

$$Z_r = \frac{1}{\Lambda} \tag{1.54}$$

Usually this simple equation does not reproduce an accurate result. In 1994 Haas et al [23]. proposed a more accurate equation for the Z_r calculation,

$$Z_r = \frac{3\zeta_r(5 - 2\omega + \zeta_r)}{(3 + \zeta_r)(5/2 - \omega)(5/2 - \omega + \zeta_r)\left(1 - \left(1 - \frac{\zeta_r\Lambda}{5/2 - \omega + \zeta_r}\right)^2\right)} \tag{1.55}$$

in which ζ_r is the number of rotational degree of freedom. Previously in 1959 Parker J.G. [24] calculated the rotational and vibrational relaxation collision numbers for some gases composed of diatomic molecules. For the rotational relaxation collision number he obtained the equation below

$$Z_r = \frac{Z_r^\infty}{1 + \frac{\pi^{3/2}}{2}\left(\frac{T^*}{T}\right)^{1/2} + \left(\frac{\pi^2}{4} + \pi\right)\left(\frac{T^*}{T}\right)} \qquad 1.56$$

and for Z_r^∞ and T^* he proposed the following values for oxygen and nitrogen.

Gas	Z_r^∞	T^*
N$_2$	15.7 collisions	80 K
O$_2$	14.4 collisions	90 K

Table 1.1. Values for the rotational relaxation collision number [25].

The values stated in Ref. [25] may regarded appropriate for hard sphere molecules and an overview of generalizations to other molecular models found in [26] and [27] proposed an extension to the variable hard sphere model,

$$Z_r = \frac{Z_r^\infty}{1 + \frac{4\pi}{3}\frac{\Gamma(3-\omega)}{\Gamma(7/2-\omega)}\left(\frac{T^*}{T}\right)^{1/2} + \frac{2(\pi^2/4+2)}{5/2-\omega}\left(\frac{T^*}{T}\right)} \qquad 1.57$$

where Γ is the gamma function. A generalization to the variable soft sphere model was presented by Koura et al. in 1996 [28],

$$Z_r = \frac{\frac{m}{2m_r}Z_r^\infty}{\frac{5/2-\omega}{1+a} + \frac{\pi^{3/2}}{2}\frac{\Gamma(1+a)}{\Gamma(3/2+a)}\frac{\Gamma(3-\omega)}{\Gamma(5/2-\omega)}\left(\frac{T^*}{T}\right)^{1/2} + (\pi^2/4+2)\left(\frac{T^*}{T}\right)} \qquad 1.58$$

which also considers collisions between different types of molecules. It must be noted that the symbol ω represents the exponent in the viscosity-temperature law. In literature generally also the VHS parameter $\xi = \omega - 1/2$ is denoted by ω, hence the equation above may appear differently in different sources.

1.5 Surface Interactions

Several years ago Maxwell proposed two fundamental models for the interaction of a stationary gas with surfaces in equilibrium, namely diffuse reflection and specular reflection. In specular reflection the velocity component normal to the surface is reversed while the tangential velocity remains unchanged. Thus a specular reflecting boundary is perfectly elastic and acts as a plane of symmetry. In diffuse

reflection the post-reflection velocities of the molecules are independent of the velocities before the surface interaction, and they are distributed according to the Maxwell distribution. For equilibrium diffuse reflection the temperature corresponding to the Maxwell distribution of the reflected molecules and the surface temperature need to be equal to the gas temperature. However, in practical applications the gas molecules generally have a stream velocity relative to the surface that is not zero and thus the gas near the surface is not in equilibrium. A useful generalization of the equilibrium diffuse reflection model is obtained by considering different temperatures for the incident molecules T_i and the wall T_w and allowing exchange of energy such that the temperature of the Maxwell distribution of the reflected molecules T_r is equal to the wall temperature T_w. In the following this gas-surface interaction model is referred to as completely diffuse reflection with full accommodation to the surface temperature [1].

In real flows the extent, to which the reflected molecules have adapted their temperature to that of the surface, may be measured by the thermal accommodation coefficient

$$a_c = \frac{q_i^" - q_r^"}{q_i^" - q_w^"}$$
1.59

In this equation $q_i^"$ and $q_r^"$ are the incident and reflected energy fluxes respectively, and $q_w^"$ is the hypothetic energy flux that would leave the surface by diffuse reflection and complete adaption of the molecules to the wall ($T_r = T_w$). Similarly the accommodation coefficients of the normal and tangential momentum could be defined.

The simplest approach to modeling the partial accommodation effects is to consider a fraction a_d of the molecules to be reflected diffusively and specular reflection for the other molecules. A more elaborate phenomenological model for incomplete accommodation was developed by Cercignani, Lampis and Lord and is explained in detail in Ref. [1]. The CLL model includes separates accommodation coefficients for the normal energy and tangential momentum and is therefore superior to diffuse-specular reflection.

Experiments with gases in contact with surfaces showed that the reflection behavior is well approximated by the diffuse-reflection model with complete thermal accommodation for the majority of practical problems. Therefore, this boundary condition is used more often in numerical studies. However, in certain cases the thermal accommodation can be significantly lower than unity and Bird in [1] mentions three conditions under which the assumption of full adaption to the wall temperature needs to be carefully validated :

- Smooth metal surface that has been outgassed by exposure to high vacuum
- Small ratio of the molecular weight of the gas to that of the surface molecules
- Very high translational energy of the gas molecules relative to the surface

In this study none of these issues clearly applies so the diffuse reflection with full accommodation to the surface temperature is employed in all calculations. Usually for polyatomic molecules additional coefficients for the accommodation of internal modes need to be specified. In the cases discussed below only rotation is considered and the corresponding accommodation coefficient is set to unity. Hence the velocity and rotational energy of the reflected molecules are both sampled from their equilibrium at the surface temperature.

The SPARTA kernel

2.1 Introduction

The name SPARTA stands for Stochastic Parallel Rarefied-gas Time-Accurate Analyzer. The code is developed in Sandia Laboratories by M.A. Gallis and S.J. Plimpton [2] and is distributed as an open source code under the terms of the GPL license. It is written in a way to be easy to extend, modify or add extra functionality. The code can run on a single processor as well as on a cluster of processors using the MPI library and domain decomposition of the simulation domain. Although its robustness and flexibility the code is not addressed to non-experienced users. It requires an understanding of the DSMC method and a specifically written input script in order to be able to run a simulation. SPARTA executes by reading the commands in the script line by line [29].

The input script must have a specific structure in order for the code to be able to read it. It is divided in four parts:

1. Initialization
2. Problem definition
3. Settings
4. Run a simulation

The third and fourth section can be repeated until convergence is achieved. In this section we will describe each part of the input script in detail as well as some important features of the code.

2.1.1 Initialization

In this part of the input script we set the parameters for the simulation. These parameters include the units of the simulation (CGS or SI), the initial seed for the random numbers generator and the dimensions of the problem, 2 for 2d and 3 for 3d simulation domains.

2.1.2 Problem definition

In the problem definition section we define all the parameters needed for the simulation to begin. Typically this parameters are the coordinates of the simulation box, the grid that will be used for the simulation, surfaces that are inside the simulation box, our particle species and the initial population of the particles. The coordinates of the faces of the simulation box. In a 2d simulation or domain is a rectangle with four faces one in the minimum of the x-axis, one in the maximum of the x-axis and the same happens for the y-axis. On a 3d simulation we have two more faces in the minimum and maximum position of the z-axis.

Regarding the simulation grid SPARTA uses an hierarchical Cartesian grid [29]. This means that the whole simulation domain is considered a single parent grid cell at level 0. Then this cell is divided in N_x by N_y by N_z cell at level 1. Each of these cells can be a child cell (no further division) or a parent cell further subdivided by N_x by N_y by N_z cells at level 2. In such grids we can have up to 16 level of subdivision in 64-bit architectures. As stated above SPARTA uses domain decomposition in order to run a simulation in parallel. This means that each processor gets a small portion of the entire domain, apply the algorithm

routines and then communicating with its neighbors in order to exchange particles. Each processor has a copy of all parent cells. As far as child cells are concerned every processor has its own child cells.

Child cells can be assigned to processors using one of these four methods, clump, block, stride and random. The clump and block methods lead to geometrically compact processors as they create clump assignments of child cells in each processor [29]. The stride and random methods produce dispersed assignments of child cells to every processor. By using the clump method we assign the Pth cell to the same processor. This means that each processor gets the same portion of the simulation domain. In e.g for a domain with 10000 cells and 100 processors, the first processor will get the cells from 1 to 100, the second from 101 to 200 etc. The block method creates a virtual logical grid of processors that overlays the simulation domain and each processor is assigned a contiguous block of cells. In the stride method every Pth cell is assigned to the same processor, where P the number of processors. Using the same example as above with a grid of 10000 cells and 100 processors, with the stride method the first processor will be assigned the cells 1,110,210...9100 whereas the second will get the cells 2,102,202...9200, and so on. Finally the random method means that each grid cell will be assigned randomly to one of the processors. In this case not all processors have the same number of grid cells.

In this section of the input script we can also specify if the system will be load-balanced. The load balancing performed at the beginning of the simulation is static since it is performed once. At this stage we attempt to balance the computational load evenly across processors. After the grid has been created and the grid cells are assigned to the processors, then they are migrated to their new processors together with the particles they own. As an addition to the above SPARTA also has a gridcut feature which if used correctly optimizes the simulation time.

Gridcut can be applied to a clump assignments only. In the domain decomposition method each processor stores information about the ghost cells of its neighbors. By using gridcut we determine at which distance the ghost cell information will be stored [29]. For example if gridcut is defined as -1 then each processor will store a copy of all ghost cells used in the simulation. This will consume a lot of memory if simulating a big system. In addition if gridcut is 0 then each processor will store a minimal number of ghost cells. Whereas this will consume less memory it requires more messages to be passed in order to move the particles into their new processors which might create a bottleneck in processors communication. In the cases presented below a gridcut value of 3 level-2 cell diameters was used in order to avoid communication

After the initialization and problem definition parts have been completed it is time for the settings part of the input script. In this part we define the outputs of the simulation, the collision model, the chemistry model, dynamic load balancing, boundary conditions, surface reflection models etc. This part of the script is of extreme importance as it will define the quality of the simulation results as well as the speed of the simulation. More specifically in this part we define the simulation timestep, the variables of the flow field that will be computed, the computation of surface properties and our sampling intervals. Finally after all these have been defined properly we set up our output intervals. As stated above this part is very important because a miscalculation in the sampling intervals or writing output results too often can slow down our simulation speed.

Furthermore in this part is where we define how our dynamic load-balancing will be performed. In order to perform dynamic load-balancing SPARTA adjusts the assignments of grid cells and their particles to each processor in order to attempt to spread evenly the computational load. After performing dynamic load-balancing the cells assigned to each processor are either clumped or dispersed. There are 3 methods in order to perform dynamic balancing in SPARTA. We can produce clumped assignments of child cells to each processor, dispersed assignments of child cells to each processor or we can use a recursive coordinate bisectioning method [29].

In more detail by using the first method each grid cell will be assigned randomly to one of the processors. But in this case not every processor gets the same amount of grid cells. In the second case each processor selects randomly one processor to assign its first grid cell to, then it loops over its grid cells and assign each to consecutive processors. Also with this method not every processor has the same amount of grid cells after the balancing. By using a recursive coordinate bisectioning method (RCB) processors are assigned compact clumps of grid cells. In this method every cell has a weight so that each processor is assigned an equal total weight of grid cells. The weight of the grid cells can be 1.0 so that every processor gets an equal number of cells or can be the particles currently owned by the cell. In this way each processor gets an equal number of particles.

In order for SPARTA to perform the dynamic-balancing routine it requires two more arguments. An imbalance factor which is defined as the maximum number of particles by owned by any processor divided by the average number of particles per processor. The second argument is the frequency in which the imbalance of the simulation is checked [29]. These two factors must be chosen wisely in order to avoid communication overheads during the simulation. In the cases discussed later we have found that an imbalance factor of 30% worked fine and the frequency the imbalance factor was checked was no more than two times during the simulation. Exception is the flared cylinder case in which due to very large number of timesteps needed four imbalance checks were performed during the simulation.

Test Cases

3.1 Introduction

In the test cases described below an effort has been made to implement hypersonic rarefied flows in SPARTA. Four well known validation cases obtained from literature have been concerned. The first case is a hypersonic flow around a flat plate and there is a comparison with results obtained by solving this case with DAC (DSMC Analysis Code) which is NASA's production code for DSMC simulations. The results computed by DAC are obtained from [30]. The second test case is the hypersonic flow around a 70-degree blunt cone. In this case the heat transfer from the flow to the surface of the cone is measured. The last two test cases are the flow around a flared cylinder and the flow around a biconic. These two cases are characterized by complicated flow phenomena such as very steep gradients of velocity, temperature and density, shock/shock interactions, compression and rapid expansion. These phenomena make these flows very complex so that a special study on the simulation parameters has to be conducted before starting the simulation. These specific test cases have been used before in order to validate some of the very well-known parallel DSMC codes. Examples of these codes are DAC [3], SMILE [4], MONACO [5], ICARUS [6], MGDS [7], and dsmcFoam [8]. In order to obtain experimental data for the above cases, the experiments were conducted in low pressure free-jet expansion tunnels.

3.2 Flow around a flat plate

3.2.1 Introduction

Various implementations of the direct simulation Monte Carlo (DSMC) method exist in academia and industry. By comparing implementations, deficiencies and merits of each can be discovered. This test case reports comparisons between DSMC Analysis Code (DAC), Stochastic Parallel Rarefied-gas Time-accurate Analyzer (SPARTA) and DS2V. DAC is NASA's standard production code and SPARTA is a research open-source DSMC code developed in Sandia National Labs by Michael Gallis and Steve Plimpton. DS2V is a well-established DSMC code developed by Graeme Bird. In addition to DAC and SPARTA, DS2V is developed in such a way that it can be controlled interactively by the user while requiring minimal user input. In this study, DAC and SPARTA are compared with DS2V by having each simulate a flat plate wind tunnel test, using an identical mesh. Flow results are compared with available experimental data. Overall, this study revealed that both codes, have interesting differences. For parallel processing, DAC was slightly more efficient in this case whereas SPARTA is far more efficient regarding memory spread. Although DAC showed better efficiency the particles number is not large enough so that a final decision could be made. As far as results accuracy is concerned both DAC and SPARTA results are compared also with DS2V which is a well-established and accurate DSMC code.

This chapter begins by providing a brief overview of DAC. Then a description of their setup for comparisons is given. Regarding DS2V a description of its setup is not provided due to the fact that DS2V requires only the flow conditions and the surface geometry. The mesh manipulation in DS2V is done by the code itself

and no user input is required. Next, a description of the flat plate wind tunnel test is provided. Afterwards the boundary conditions and collision model configurations are outlined.

Following these descriptions, comparisons of resulting flat plate simulations are presented. First, serial and parallel simulation time and memory are compared. Second the quality of the simulations is examined through DSMC metrics. Third, flow field contours of macroscopic flow properties are discussed. Finally, surface properties are studied, including comparison against existing surface pressure and heat flux data found in literature. Finally we have to mention that as DAC use is restricted outside US the results of the DAC code were taken from a NASA Technical Report [30].

3.2.2 Description of DAC code and SPARTA applications

DAC was invented in the mid 1990's by LeBeau and others [3] [31]. The code is written in FORTRAN 77, and uses Cray style pointers to permit dynamic memory allocation. DAC has been employed by NASA and other organizations for mission support, aerospace vehicle design analysis, computational nonequilibrium gas modeling and in support of laboratory projects [32]. Simulations have involved nonequilibrium flow around spacecraft in orbit [32], [33], [34] rarefied hypersonic flow [35], [36] and support of hybrid simulation research [32], [36]. For DAC the computational grid is a composition of a surface grid and a flow-field volume grid. By using two grids, the surface grid does not impose a geometric constraint on the surrounding volume grid. The surface grid, generated independently, is a closed surface comprising an unstructured distribution of triangular cells. The flow-field grid is generated automatically by DAC's preprocessing utility called PREDAC. It is nominally bounded by six planes, each coordinate axis perpendicular to a pair, and by the surface grid. Each bounding plane represents an inflow, outflow or symmetry boundary. Alternatively, the computational domain can be defined more generally via the use of the same type of unstructured triangular grids that are used to define a surface, as the boundary conditions for these grids can be defined as surface, inflow or outflow. The initial flow-field grid comprises three-space Cartesian cells, labeled "level 1" cells, often distributed uniformly along each coordinate direction for initial simulation. Solution results obtained from level 1 cells enable PREDAC to refine the grid in regions of higher flow density by dividing level 1 cells into smaller cells, labeled "level 2" cells.

On the other hand SPARTA is a fairly new code and its applications portfolio is very limited. Besides that, the code has been used to conduct two very difficult and computational intensive simulations. The first one was the flow around the Mir space station at an altitude of 300K feet [37] and the Richtmyer/Meshkov mixing problem [38]. In the first case around 1.6 billion particles and 2048 cores were used whereas in the second 4.5 billion particles and 512K cores where used. These two large applications witness that SPARTA can be used in massively parallel machines.

3.2.3 Description of flat plate simulations

For this study, comparisons are achieved by simulation of rarefied flow about rectangular flat-plate model within a free-jet expansion wind-tunnel. The particular geometry and flow conditions are taken from an experiment presented by Allègre and others in 1992 [12]. This experiment is characterized by a rarefied global Knudsen number of 0.016 based on the free stream mean-free-path $\lambda = 1.6mm$ (computed from free-stream conditions) and flat-plate length $L = 100mm$. Flat plate thickness is $5mm$. Identical flow

conditions are employed to simulate the experiment. Flow commences with a vacuum domain. Inflow of pure nitrogen is assumed. The following input parameters define the nitrogen gas species: molecular weight $MW = 28.01$, VHS molecular diameter $\delta_{diameter} = 4.17 \times 10^{-10} m$[13] viscosity index $\omega = 0.74$, at reference temperature $T_{ref} = 273\ K$[13] and a number of rotational degrees of freedom $\zeta_{rot} = 2$. Simulations are performed with molecule rotational energy exchange procedures activated. Nitrogen gas enters the inflow boundary uniformly with $V_\infty = 1504 m/s$, $T_\infty = 13.32\ K$, and $n_\infty = 3.716 \times 10^{20}\ m^{-3}$. Free stream velocity is parallel to x axis and longitudinal surfaces of flat plate. The flat plate boundary condition is an isothermal wall temperature $T_w = 290\ K$. Gas molecules are assumed to reflect diffusively from the wall according to the Maxwellian velocity distribution at T_w .

The computational flow field grid selected for baseline simulation is a two-dimensional structured grid with rectangular cells having 0.5 mm sides. The simulation domain is a symmetric rectangular region of flow about the flat-plate. The domain dimensions are 180 by 205 mm in the *x* and *y* directions respectively. Inflow boundary is defined by the front face, outflow boundary is defined by the right face and reflective boundaries are defined by top and bottom faces. Flat plate surface boundary is defined by the open interior region with dimensions 100 by 5 mm in the *x, y* directions respectively. The origin of the coordinate system is set at the center of the flat plate left face. Flow field mesh was generated with level 1 cells.

In order to determine the cell size, the rule of "one third of mean free path" was used. The free stream mean free path for these conditions is 1.6 mm so the cell size is slightly smaller than the one third of the mean free path.

3.2.4 Comparison of Flat Plate Simulations

In order to be able to compare simulations, the same simulation parameters listed in the report are input to SPARTA and DS2V. The parameters are summarized in Table 1. In SPARTA input script we set the "stat" to 100 and the "restart" to 2000. This means that SPARTA will print the statistics every 100 steps and it will write a restart file every 2000 steps. In DS2V we have no control in the code output so it prints the statistics in every time-step.

Time-step	$3.102 \times 10^{-7} sec$
Particle weight	$4.56 \times 10^{11} real\ per\ simulated\ particles$
Transient period	$8000\ steps$
Sampling period	$8000\ steps$
Interval Sample data	2

Table 3.1. DSMC simulation parameters

DAC serial processing executable was generated with Intel® 10.1.018 compilers using default optimization [30] while SPARTA executable was generated with MPICH 3.1.3 MPICC compiler wrapper using the Makefile provided with the code with default optimizations. DS2V comes precompiled and the executable can be run directly. For SPARTA and DS2V simulation time and memory used are calculated by the code metrics whereas for DAC were taken directly from the technical report [30]. The results of serial execution are shown in Table 3.2. DAC run on an AMD Opteron™ Processor 244, which has a 1.8 GHz clock while

SPARTA run on an AMD Opteron™ Processor 6380, which has a 2.5 GHz clock. At this point we have to mention that the processor that SPARTA was run is more efficient and faster in comparison with the processor in which DAC was run. Besides that the processor is only responsible for a small percentage of the overall speedup, for the rest are the code's data structures. In our case SPARTA seems to have better data structures and management than DAC while DAC requires less memory. Although DS2V was run on an AMD FX™ 8350 which is clocked in 4.0 GHz is slightly slower than SPARTA but it has the best memory efficiency.

Simulation code	DAC	SPARTA	DS2V
Real time (hr:mm:ss)	9:42:18	3:12:10	3:36:52
memory	223 MB	328MB	213MB

Table 3.2. Serial processing simulation

The next figure demonstrates SPARTA and DAC progression towards steady-state. Steady-state begins when the number of simulation particles remains consistently within two standard deviations from sampled particles mean. SPARTA and DAC simulator particles arrive at steady-state after 1500 time-steps. The number of molecule collisions per time-step for both codes becomes steady after 1100 time-steps. During the sampling period the simulator particles in DAC simulation is 3,169,267 and 3,174,884 in SPARTA. Mean number of gas-gas and gas-solid molecule collisions in SPARTA are 46,671 and 854 respectively whereas in DAC are 50,042 and 894 respectively. These are 7% and 4.5% respectively less than DAC.
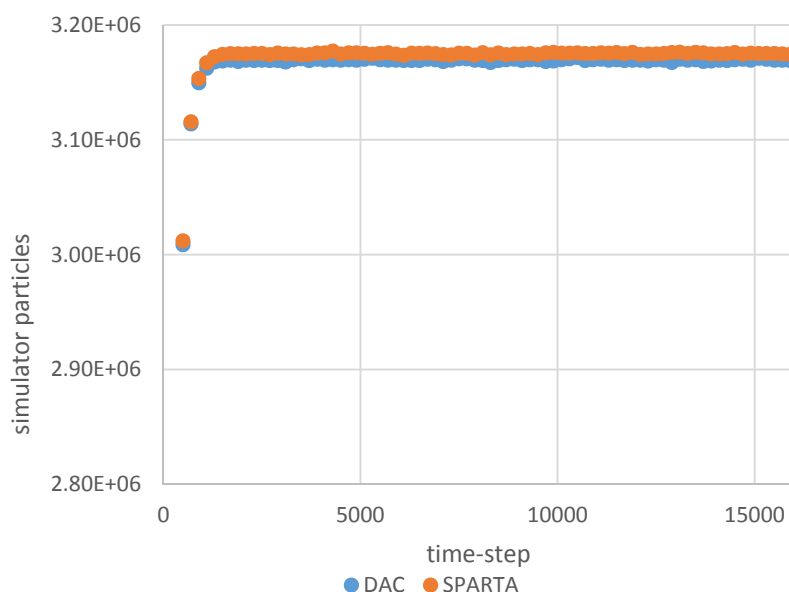
Figure 3.1. Comparison of simulator particles

Furthermore parallel processing performance is examined. As the report states in this case DAC was compiled with Intel® 10.1.018 compilers using default optimizations with Open MPI 1.2.7. SPARTA did not need any recompilation as it was compiled with MPICH 3.1.3 MPICC compiler wrapper. The selected case

is repeated with 2,4,8,16 and 32 processors. Then, we compute parallel processing speedup efficiency n_{ps} [30]and memory spread s_{pm} [30] using the equations below:

$$n_{ps} = \frac{t_s}{N_{proc}t_{parallel}}$$

3.1

$$s_{pm} = \frac{\Sigma_{proc}m_{proc}}{m_s}$$

3.2

Where t_s and $t_{parallel}$ are serial and parallel run time respectively, N_{proc} is the number of processors used for the simulation, m_s is the total memory used for the serial run and m_{proc} is the total memory of processor $proc$ of the parallel run.

As we can observe from the plots for this case DAC has a better parallel efficiency than SPARTA, but SPARTA has a remarkable memory spread using about the same memory for the serial and parallel runs. Every time we doubled the number of processors, SPARTA needed just 3 megabytes more memory from the previous run. Except the run with 16 and 32 processors where the 32 processors run required 30 megabytes more than the 16 processors run. Although DAC scales up better than SPARTA it is consumes much more memory.
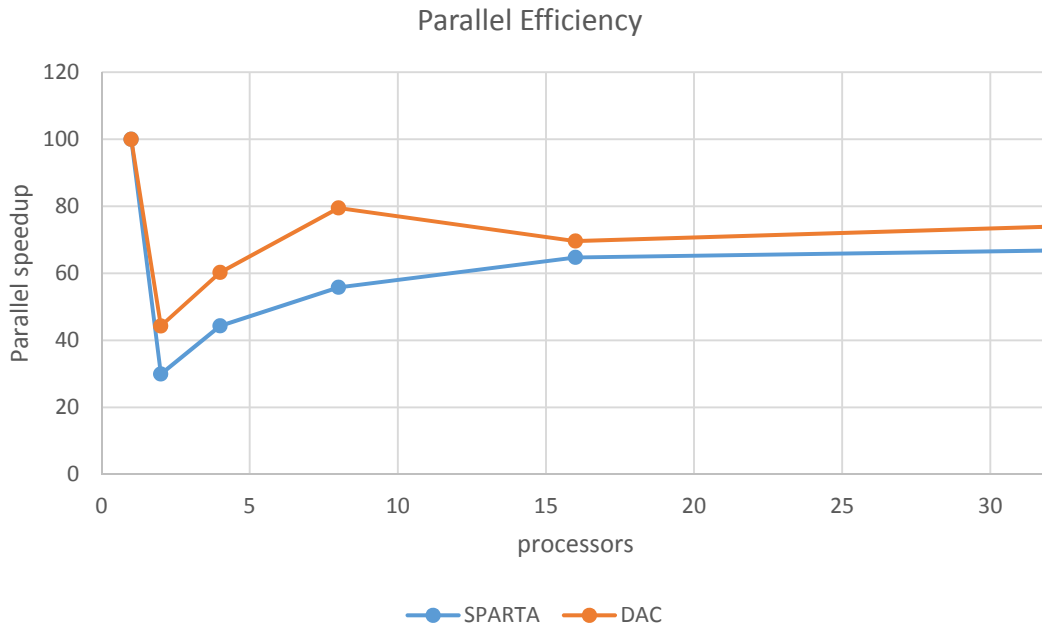
Figure 3.2. Parallel efficiency
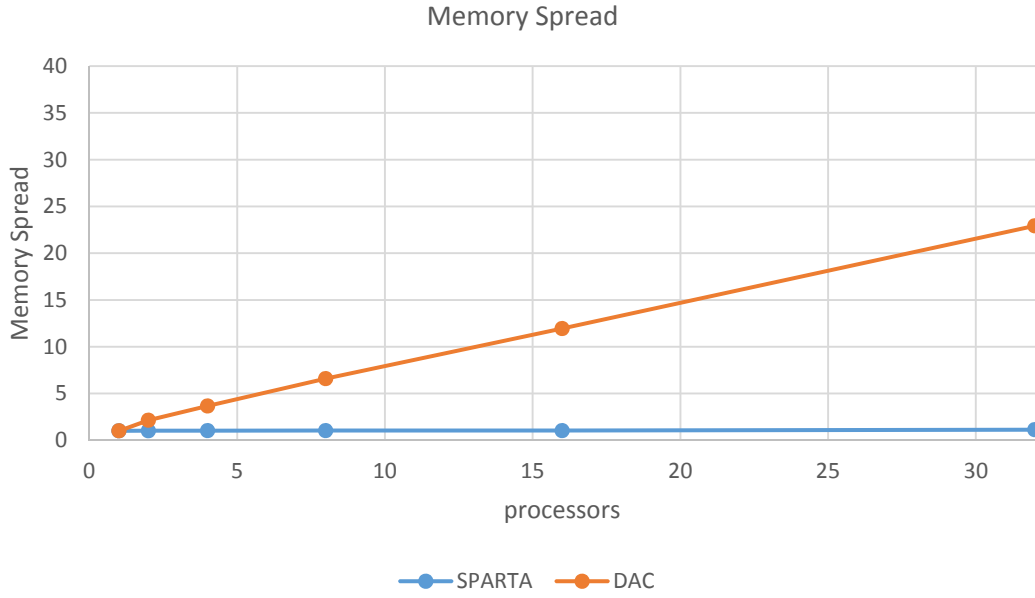
Figure 3.3. Memory spread

(a)

(b)
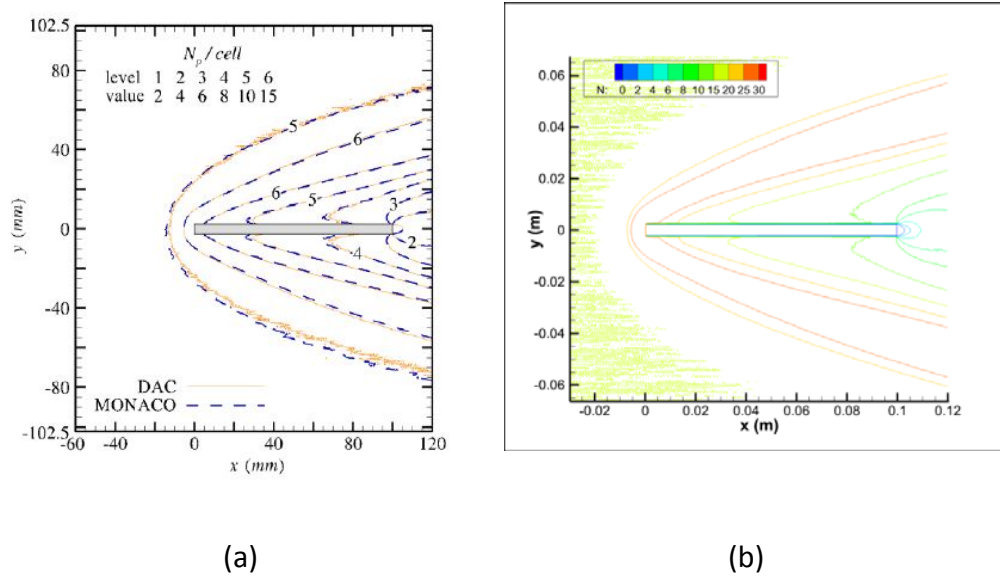
Figure 3.4. (a) Number of particles per cell DAC [30], (b) Number of particles per cell SPARTA

DSMC statistics are very important for examining the simulation statistical validity. Generally, in order for a DSMC simulation to have acceptable results the following criteria must be met: $\frac{\lambda}{\Delta s} > 1, \frac{\tau_c}{\tau_0} > 1$ and $\frac{N_p}{cell} > 10$. The present simulations obey these criteria throughout most of the computational domain. There are some exceptions in front of the plate's leading edge and behind the plate's trailing edge. The following figures compare field distribution of $N_p/cell$. In both contours the maximum number of particles is the compression regions whereas the minimum number of particles is in the wake region behind the trailing edge. Nevertheless the main difference of these sets of contours is that SPARTA has about 2 times more

31

particles per cell than DAC. As it can be seen in the report document DAC particles per cell varies from about 2-15 whereas SPARTA varies from about 4-30.
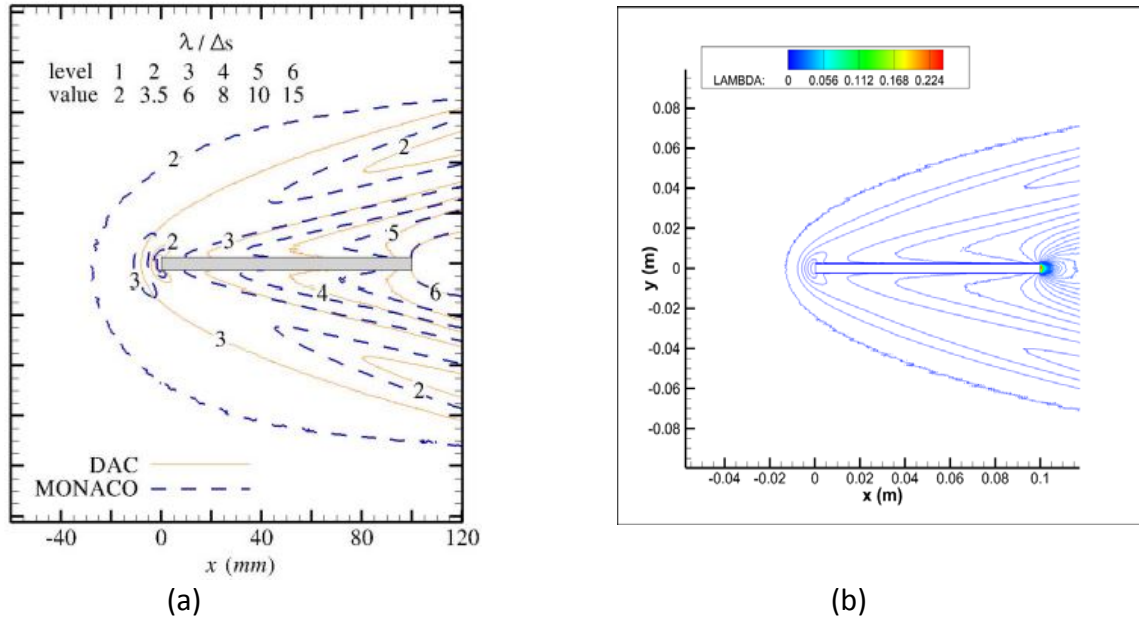
Figure 3.5. (a) Mean free path DAC [30], (b) Mean free path SPARTA

Figure 3.5 shows the mean free path that the two codes predicted. Again we observe that the mean free path around the shock area is the minimum while behind the trailing edge in the wake are we have the maximum mean free path. The differences in the mean free path numbers is because DAC uses equation 1.12a from reference [1] in order to calculate the mean free path of a molecule whereas SPARTA uses the equation 4.65 of the same reference. Although the contours of mean free path of both codes look the same we have to mention that the equation that SPARTA uses for the mean free path calculation is more accurate than DAC's. Table 3.3 summarizes the DSMC statistics results between the 3 codes.

Simulation code	DAC	SPARTA	DS2V
$\lambda/\Delta s$ $(\mathbf{min}, \mathbf{max})$	(0.55,2.59)	(0.001,0.245)	(0.00039,0.0452)
$N_p/cell$ $(\mathbf{min}, \mathbf{max})$	(0,127)	(0,250)	N/A

Table 3.3. DSMC Statistics

Next Figures illustrate the results of the flow field contours. Qualitatively, they indicate that the flow domain is adequate. Moreover the presence of a boundary layer around the flat plate, located at about $0 < x < 100\ mm$ and an oblique diffuse shock is predicted by both codes. Both code contours are in very good agreement. Similar results are observed with rotational temperature contours. In conclusion in both codes velocity and temperature contours are in excellent agreement.
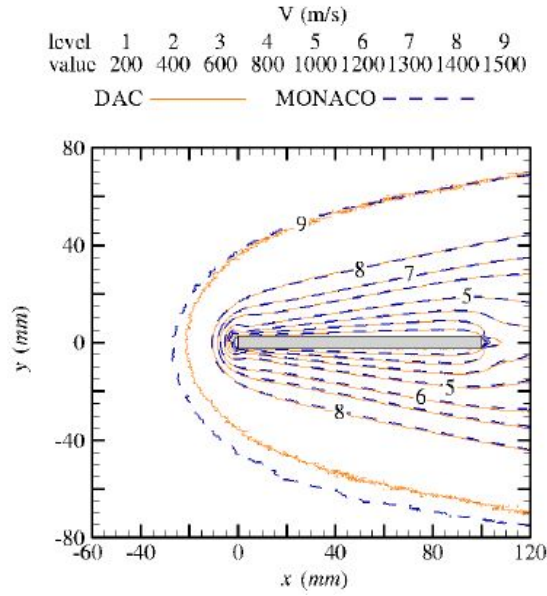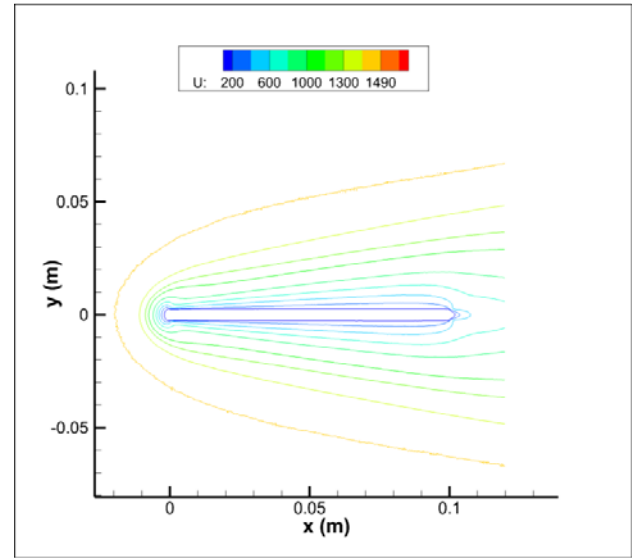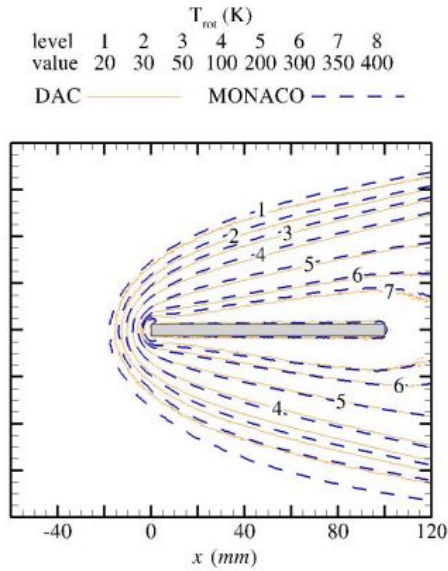
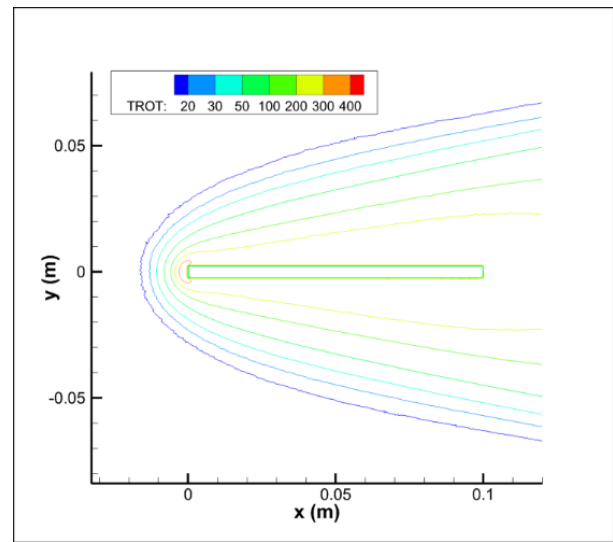(a)   (b)

Figure 3.6. (a) Velocity contours DAC [30], (b) Velocity contours SPARTA

(a)   (b)

Figure 3.7. (a) Velocity contours DAC [30], (b) Velocity contours SPARTA

The next sets of figures present the DAC, SPARTA and DS2V pressure, shear stress and heat flux along the plate's upper surface. The simulations were performed with SPARTA molecule rotational energy exchange activated as this feature produces better results. In DAC and DS2V this feature is also activated. Regarding pressure and heat flux experimental results obtained by Allègre et al [12] are included. Although there is a very good agreement between DAC, SPARTA in pressure along upper surface, DS2V is closer to the experimental results. In shear stress results it can be observed that all three codes produce very smooth

33

results. Finally there is a big difference observed in the heat flux results where SPARTA is in excellent agreement with the experimental results whereas DAC is not.
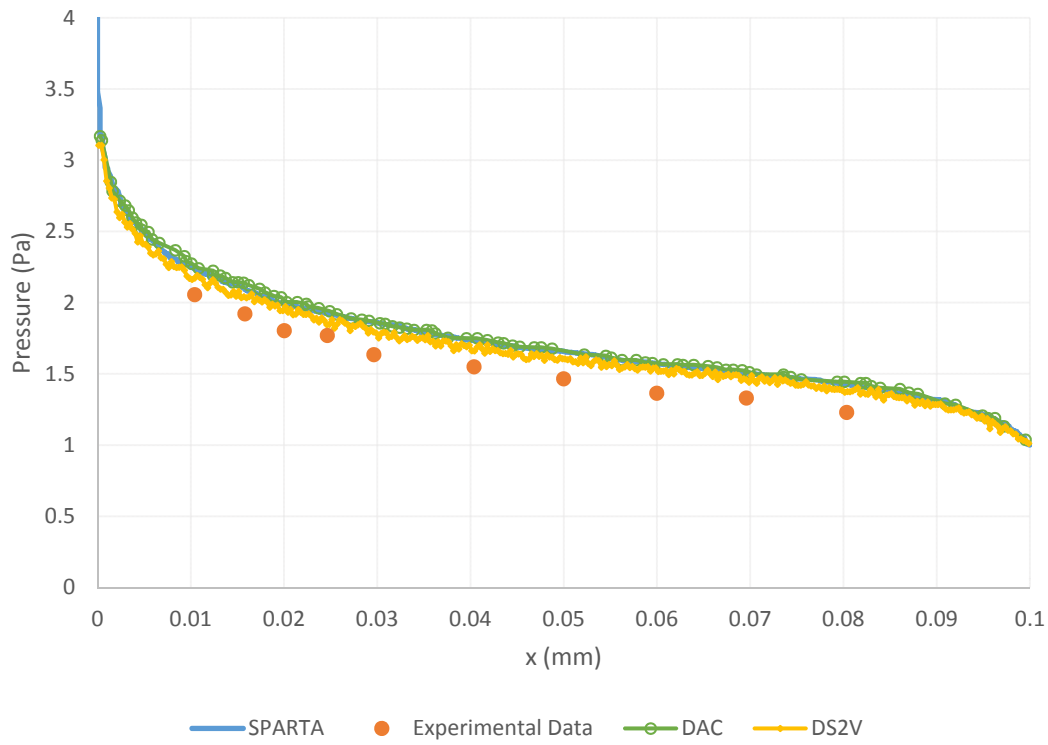

Figure 3.8. Pressure along upper surface.

In this particular test case three DSMC codes were compared. DAC which is NASA's code and SPARTA a research code developed in Sandia National Laboratories and DS2V is a legacy well-established DSMC code. SPARTA and DAC were compared using an identical domain and computational mesh, in DS2V we have no control over the mesh. Both codes show good agreement in flow field contours. In surface properties graphs all three show good agreement but with SPARTA being more accurate in the heat flux calculation and DS2V being more accurate in the pressure calculation.

Although SPARTA was about three times faster than DAC in the serial run DAC showed a better parallel efficiency than SPARTA. In addition the particles number was not so big and a study regarding parallel performance in large number of particles will be interesting. As far as memory spread is concerned SPARTA is extremely efficient as each parallel run required about the same memory with the serial run. The biggest spread was between the serial and 32 processors run were the memory required was 326 and 365 respectively. This shows that SPARTA has excellent data handling procedures within the code.

Accuracy of the simulations was in good agreement in relation with DS2V. DSMC statistics showed that both codes can produce results of good quality. Besides that SPARTA is concerned more accurate in comparison with DAC because although in pressure and shear stress was as accurate as DAC but with more smooth results in heat flux calculation it showed excellent agreement with the experimental results.

Overall this study reveals that both codes have excellent performance. DAC is little more efficient in parallel processing but with much greater memory spread than SPARTA. As far as the simulation results are concerned both have good agreement in flow field contours whereas SPARTA is more accurate in surfaces properties calculation. DS2V was used as a reference and this study revealed that both codes produce similar results to DS2V except in the heat flux calculation where SPARTA is the most accurate. The results of DAC were obtained from Ref. [30] by using a graph data extractor.
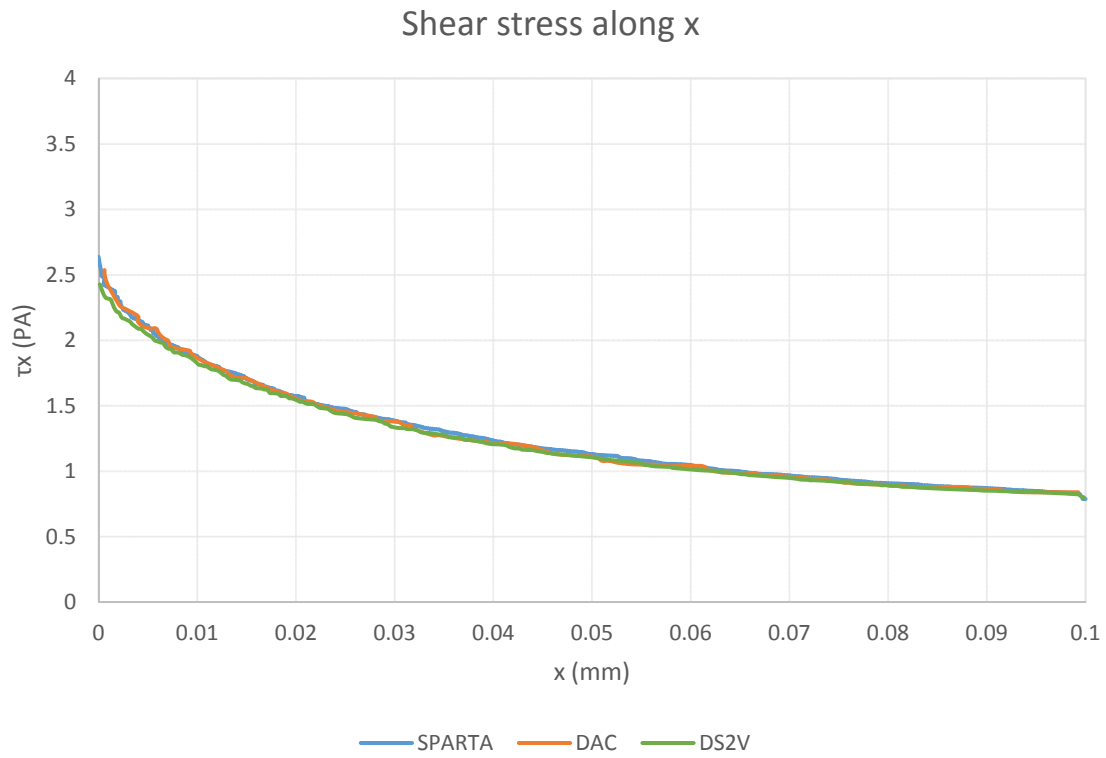
Figure 3.9. Shear stress along x.
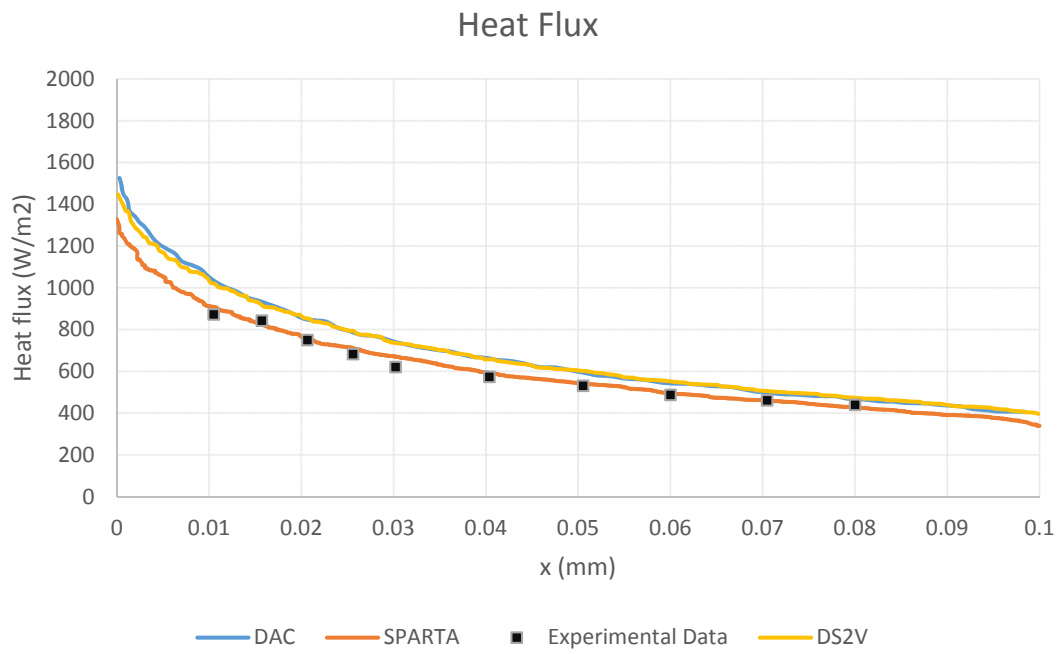
Figure 3.10 Heat Flux.

3.3 Flow around a 70-degree Blunt Cone

3.3.1 Introduction

In this test case we examine the hypersonic flows produced by a 70-degree spherically blunted cone. This cone has the same configuration as the Mars Pathfinder Probe. The blunt body/wake flow problem is one of the fundamental hypersonic problems studied computationally and experimentally by the AGARD Working Group 18 [39]. In this type of studies the most important effect studied is the influence of rarefaction and real gas effects on the near wake, in the afterbody heating and pressure distributions. In order to obtain experimental results, experiments have been conducted in low density wind tunnels and impulse tunnels. This test case have been studied in literature with both DSMC and Navier-Stokes methods [40].

As several different flow conditions exist for this test case we will focus on the first two test conditions as mentioned in Ref. [13]. These conditions were chosen because they are suitable for DSMC simulations as the pressure is small enough. The third set of flow conditions is more appropriate for Navier-Stokes simulations and it will not be used in this case. The model used in this study is the one used in the SR3 wind tunnel experiments. The model is showed in Figure 3.11 and it consists of a 50mm 70-degree blunt forecone with nine thermocouples on its surface. The positions of the thermocouples are shown in Figure 3.12. These particular sets of test conditions, both involve flow separation, due to expanding flow in the near wake of the blunted cone. Finally comparisons are presented of calculated and measured results for the heat transfer from the flow to the surface of the model.
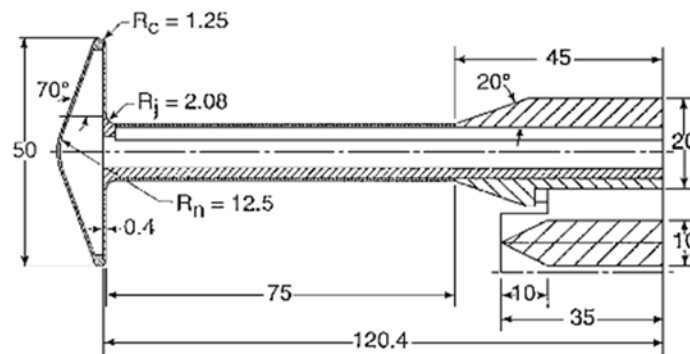

Figure 3.11 Planetary probe geometry. All dimensions are

in millimeters [13].

3.3.2 Description of the 70-degree blunt cone simulation

In this test case a test model proposed by the AGARD GROUP was used. The model is a 70-degree blunt cone mounted on a stick as seen in figure 3.11. The forebody of the model is identical to that of the mars pathfinder reentry vehicle. Experimental results were obtained from Allègre et al [13], [14] who conducted experiments in the SR3 low-density wind tunnel. During these experiments the density flowfields, drag coefficients and surface heat transfer were measured. In this test case two different grids were used. For

the first case a Cartesian uniform grid with 600 cells in the x-axis and 600 cells in the y-axis, and a two level Cartesian grid with a refinement of 10 by 10 cells along the cone's body. For the second case a finer uniform grid than the first case was used, with 850 by 850 cells. The experimental flow conditions and the experimental results are shown in tables 3.4 and 3.5 respectively whereas the simulation flowfield parameters are shown in table 3.6. Due to the symmetry of the problem the flow was modelled as 2d axisymmetric. Moreover a grid close-up of the refined grid is presented in figure 3.13 which shows the refined area of the flowfield.
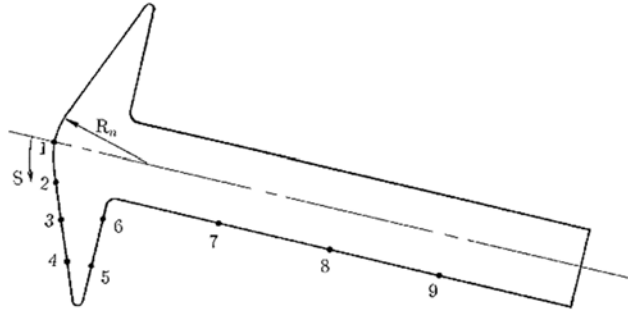
Figure 3.12 Thermocouple positions [13].

Flow conditions	Gas	Ma	T_0, K	$p_0, bars$	Re_d	$\bar{V}$
1	N_2	20.2	1100	3.5	1420	0.53
2	N_2	20	1100	10	4175	0.31
3	N_2	20.5	1300	120	36265	0.11

Table 3.4. Experimental flow conditions [13].

Thermocouple	S/R_n	$q, KW/m^2$			
		$a = 0\ deg$	$a = 10\ deg$	$a = 20\ deg$	$a = 30\ deg$
1	0	10.23	9.89	7.59	6.60
2	0.52	8.39	8.07	6.78	5.81
3	1.04	6.33	6.93	6.93	5.72
4	1.56	5.12	6.63	7.53	7.23
5	2.68	<0.02	<0.02	<0.02	<0.02
6	3.32	<0.02	<0.02	<0.02	<0.02
7	5.06	0.13	0.20	0.33	0.59
8	6.50	0.33	0.46	1.22	2.04
9	7.94	0.43	0.82	1.58	2.70

Table 3.5. Experimental results [13].

Time-step	$1.3 \times 10^{-7} sec$
Particle weight	$7.2 \times 10^{16} real\ per\ simulated\ particles$
Transient period	$100000\ steps$
Sampling period	$20000\ steps$
Interval Sample data	2

Table 3.6. Simulation parameters.

3.3.3 Results

In this section the results from solving the case are presented. Emphasis is given on the surface quantities calculated during the simulation. As it can be evidenced from the figures the flow expansion around the corner of the cone produces orders of magnitudes reductions in surface quantities with respect to their forecone values. Specifically the heating rate along the base plane, is two orders of magnitude less than the forebody stagnation point. In order to plot the results we calculate the term s, which is the cumulative distance from the stagnation point as shown in figure 3.12. The R_n term is the cone radius, which in this case is 25mm. A very good agreement is evidenced between the experimental stagnation point heat transfer and the calculated one. In table 3.6 the experimental and calculated results are presented for the uniform and for the refined grid. In figure 3.13 a close-up of the refined grid in the base of the forecone can be seen.

	$q\ (KW/m^2)$		
s/R_n	Experimental	Uniform grid	Refined grid
0	10.23	10.2281	10.2042
0.52	8.39	8.39273	8.50025
1.04	6.33	6.97913	6.99543
1.56	5.12	6.62745	6.66775
2.68	<0.02	0.002435	0.00420179
3.32	<0.02	0.002079	0.00257811
5.06	0.13	0.115016	0.12904
6.50	0.33	0.284723	0.299068
7.94	0.43	0.363092	0.368438

Table 3.7. Comparison of experimental and calculated results (case 1).

	$q\ (KW/m^2)$	
s/R_n	Experimental	Uniform grid
0	17.16	18.0031
0.52	13.56	14.666
1.04	10.24	12.1442
1.56	9.64	11.3552
2.68	<0.04	0.0377982
3.32	<0.04	0.0362018
5.06	0.43	0.429834
6.50	0.99	0.908662
7.94	1.75	0.99334

Table 3.8. Comparison of experimental and calculated results (case 2).

As it can be seen on the table above the results obtained from the uniform mesh are slightly better than the results from the refined. The reason for this is that the number of particles is not so large and by refining each coarse grid cell by 10 by 10 level-2 cells in the area of the forecone where the gradients of the flow are too steep, produces fluctuations in the sampling of flow properties as each level-2 cell has a small number of particles. In addition in the area around the back of the cone where there are not big changes in the flow gradients that's why the refined grid produces a better result. As it can be seen in the table above the heat transfer in the positions 4 and 5 could not be measured accurately due to the rarefaction of the flow. That's why the heat transfer was only characterized as being less than 0.02 KW/m^2 [41].

As far as the flowfield structure is concerned the number density increases at about four times close to the stagnation point. This is very common for hypersonic flows about cold blunt surfaces. It can also be evidenced from the number density contours that number density gradually increases as the flow approaches the forecone, indicating the diffuse nature of the shock wave that is characteristic of highly rarefied flows. As it can be seen from the velocity magnitude contours as the flow approaches the body surface at the aft corner, in the forebody a subsonic layer is developed. At the back of the cone is a recirculation area as the streamlines indicate. In the first case as it can be seen from the number density contours the density near the wake corner is about 20% more of the freestream, whereas in the second case is about 25% more of the freestream. Regarding the first case in which the flow is more rarefied than the second the vortex is not resolved very well, whereas in the second case the vortex is bigger and clearly resolved due to the less rarefaction of the flow.

In this test case two different flow conditions for a hypersonic flow around a blunt cone were studied. In the first case the gas is more rarefied than the second case, that's why some characteristics of the flow are very well resolved. Whereas on the second case due to less rarefaction the effects of the flow are very well resolved. In both cases high temperature effects are present. That yields that the nitrogen gas that surrounds the cone is in thermal nonequilibrium and one must account for the vibrational energy in order to get accurate results. The results also show that in both cases there is a formation of a vortex in the back of the cone. In the second case the vortex is bigger than the one in the first case and more accurately resolved due to the higher density of the flow. With the use of the grids mentioned above both cases have very good agreement between the experimental and the computed results. Finally must be noted that the results of the blunt cone test case are also compared with the results obtained from Ref. [9] with the use of a graph data extractor, dsmcFoam used an unstructured grid in order to calculate the surface properties.
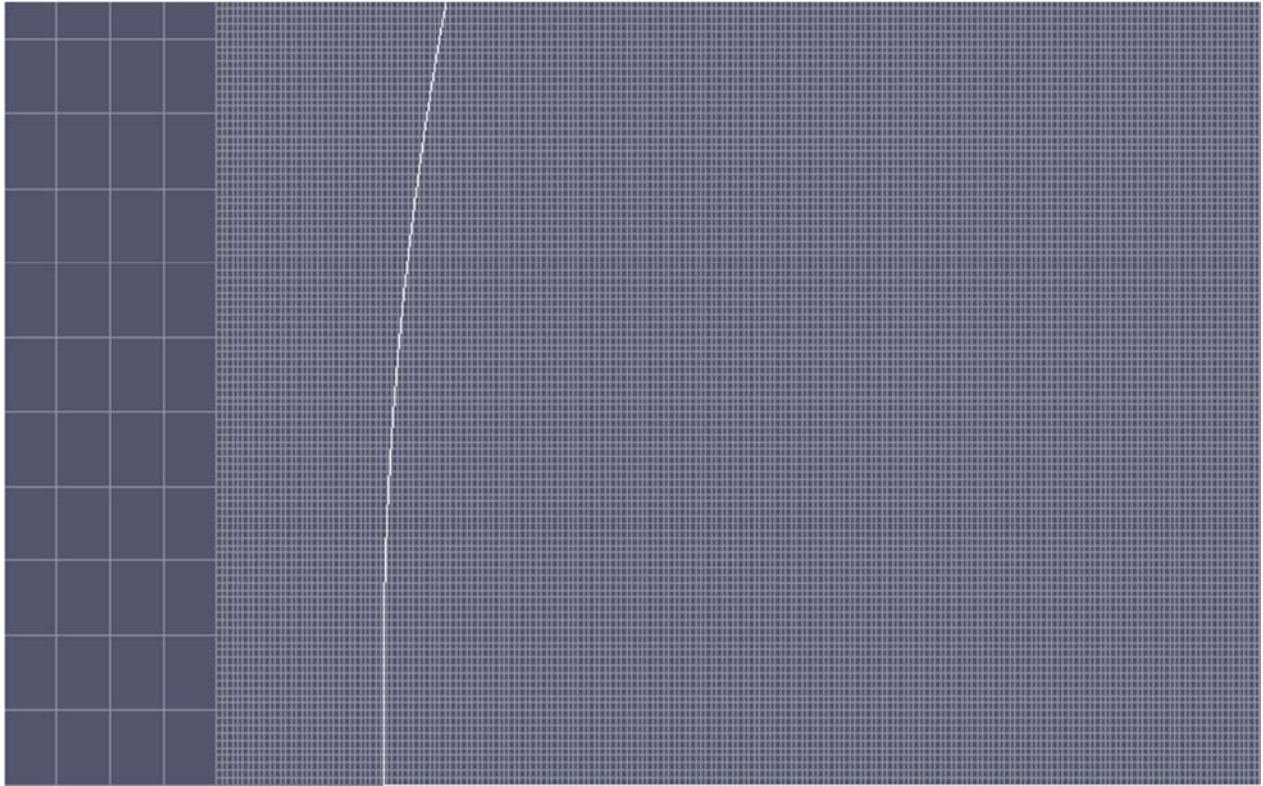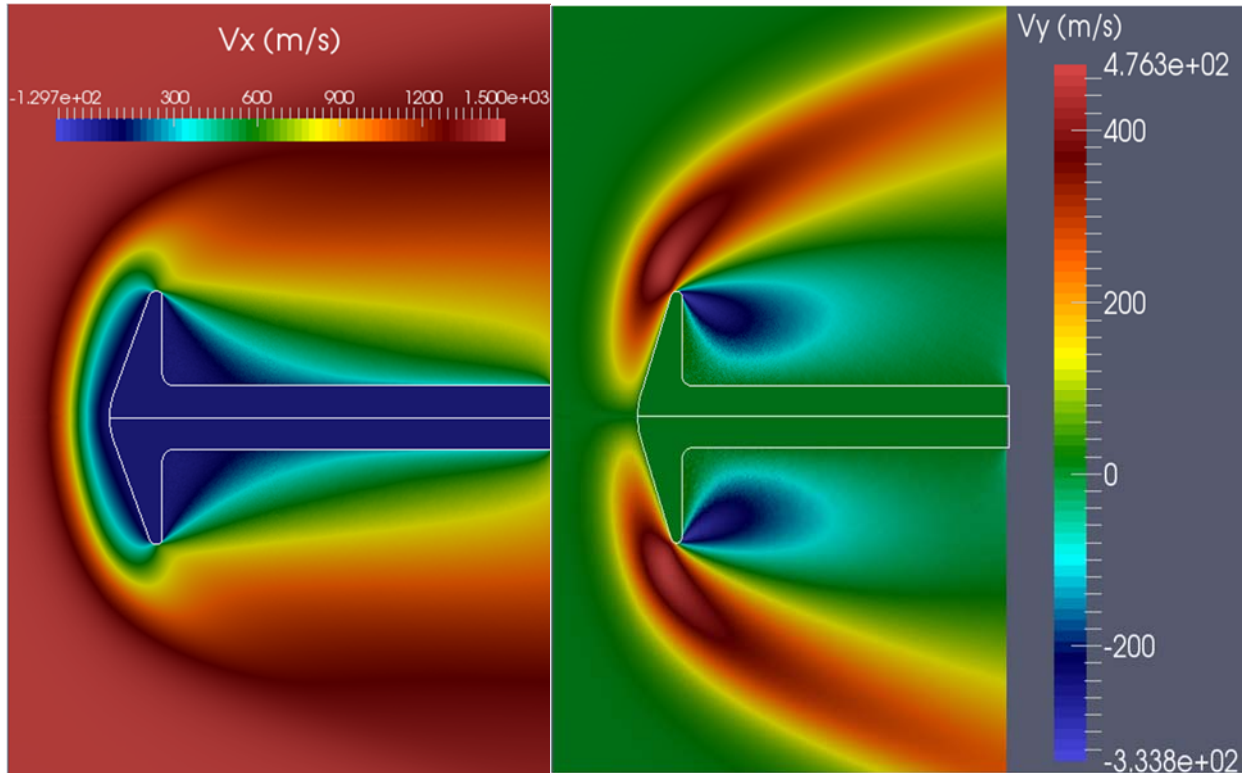
Figure 3.13. Grid close-up.

Figure 3.14. (Left) Velocity along x-axis, (Right) Velocity along y-axis (case 1).
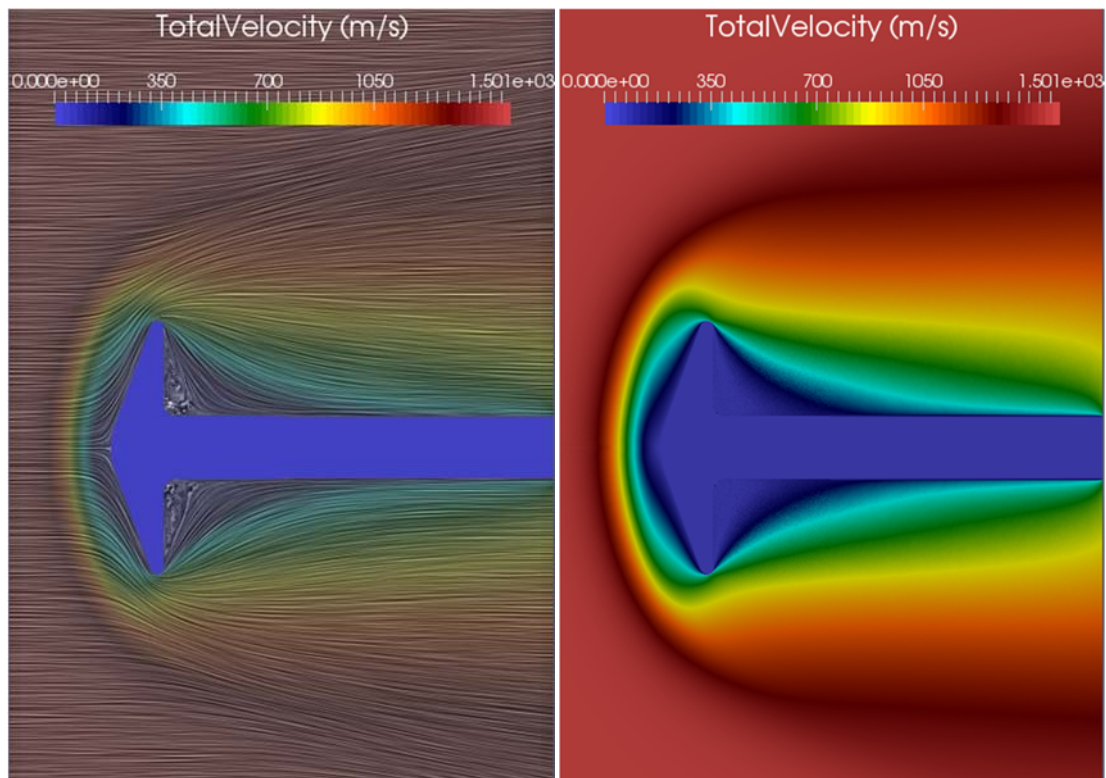
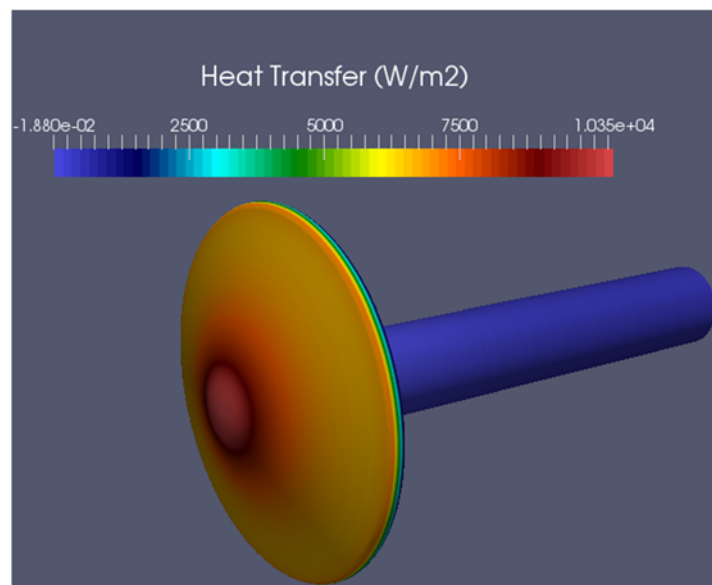Figure 3.15. (Left) Flowfield streamlines, (Right) Velocity magnitude (case 1).

Figure 3.16. Heat transfer along the cone surface (case 1).
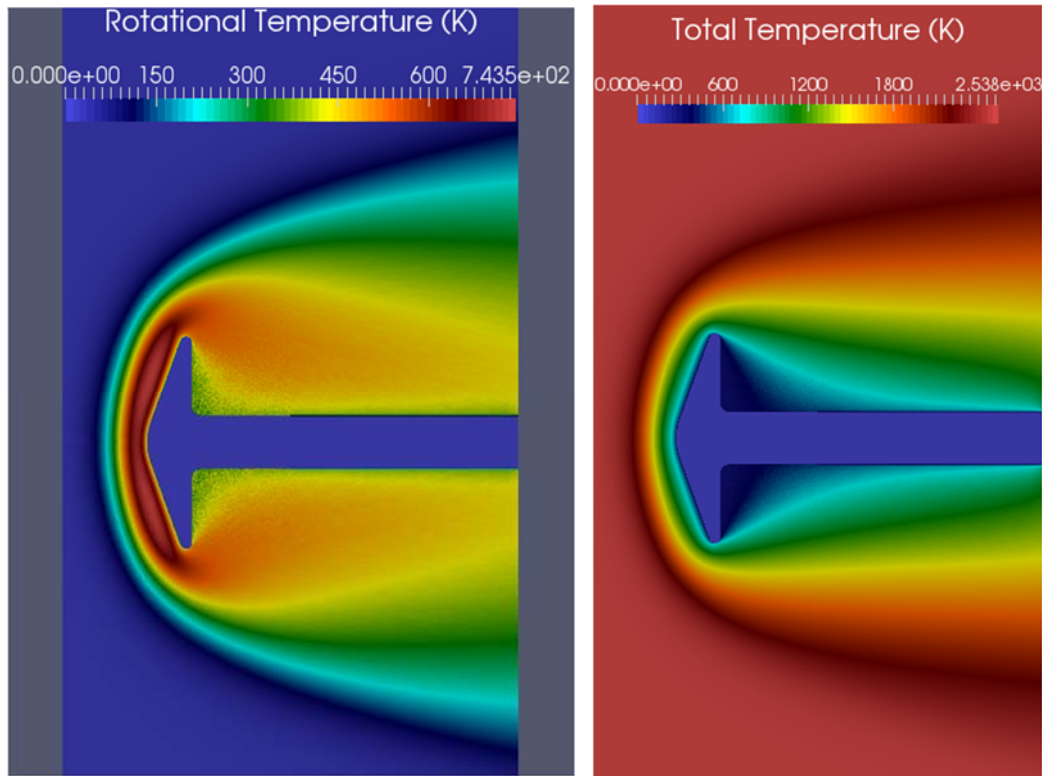
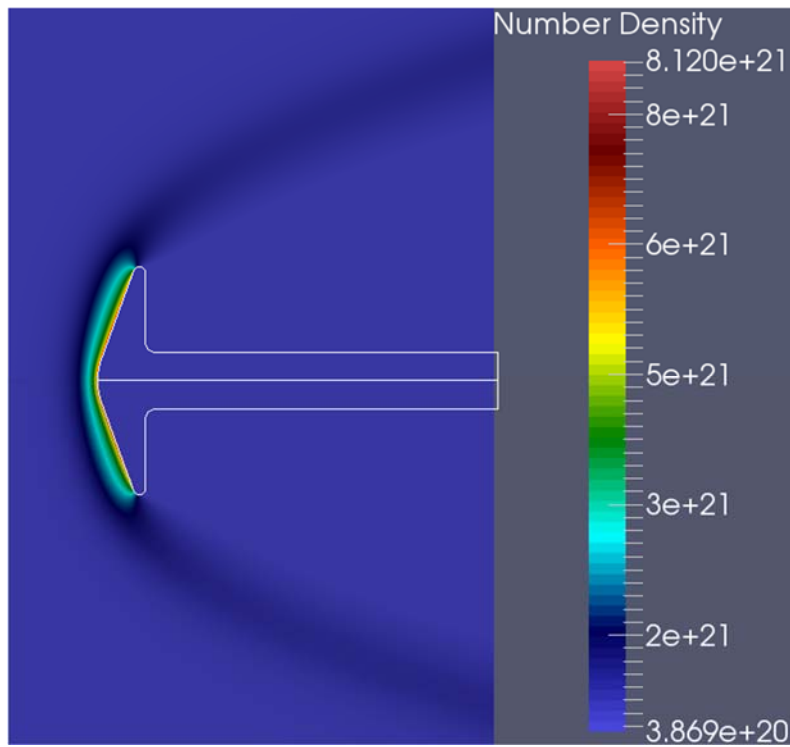Figure 3.17. (Left) Rotational Temperature, (Right) Total temperature (case 1).

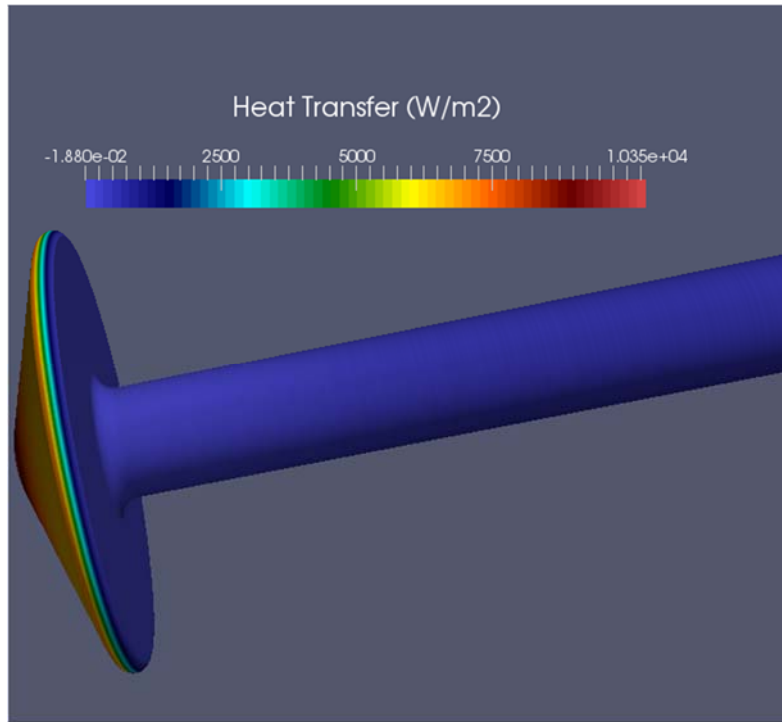Figure 3.18. Number Density contours (case 1).

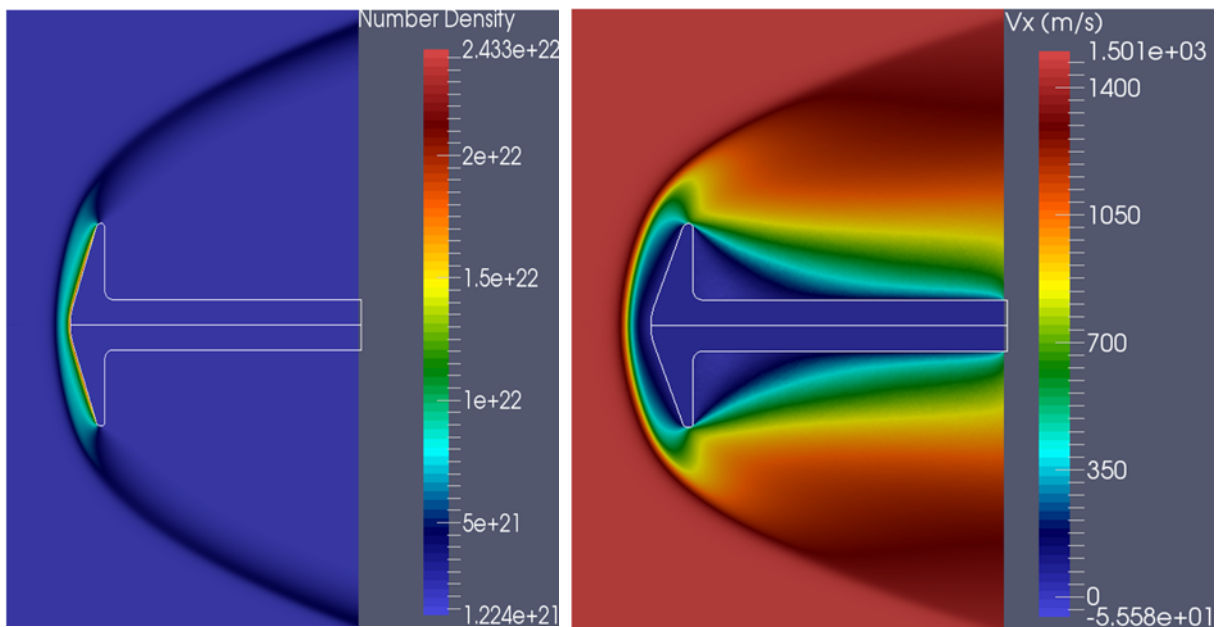Figure 3.19. Heat transfer in the backcone and the sting (case 1).

Figure 3.20. (Left) Number density contours, (Right) Velocity along x-axis (case 2).
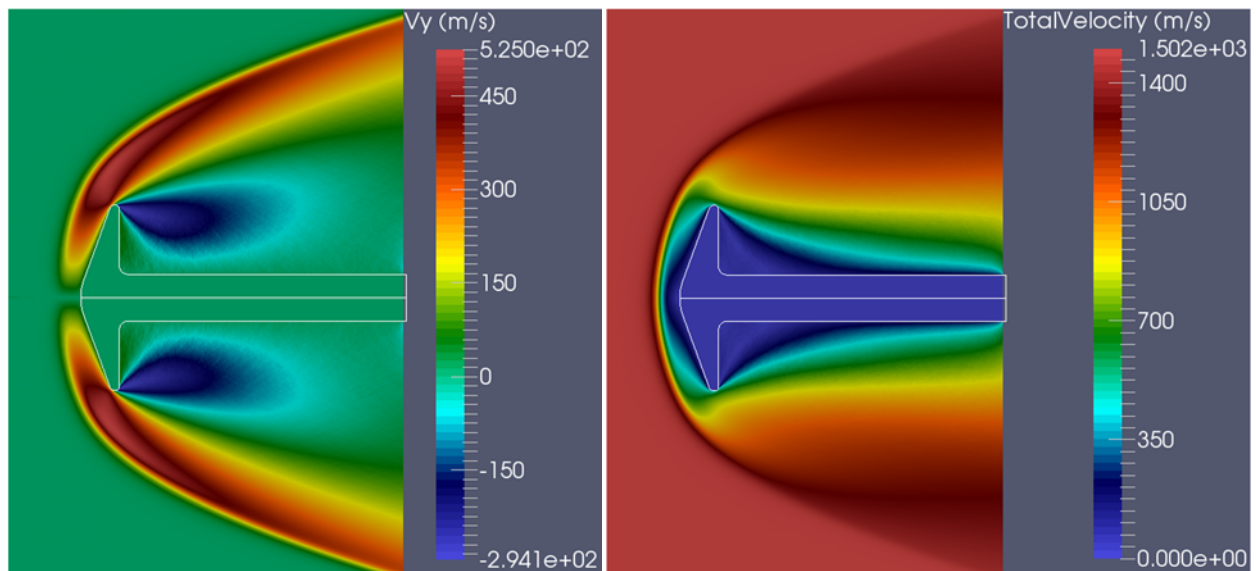
Figure 3.21. (Left) Velocity along y-axis, (Right) Velocity magnitude (case 2).
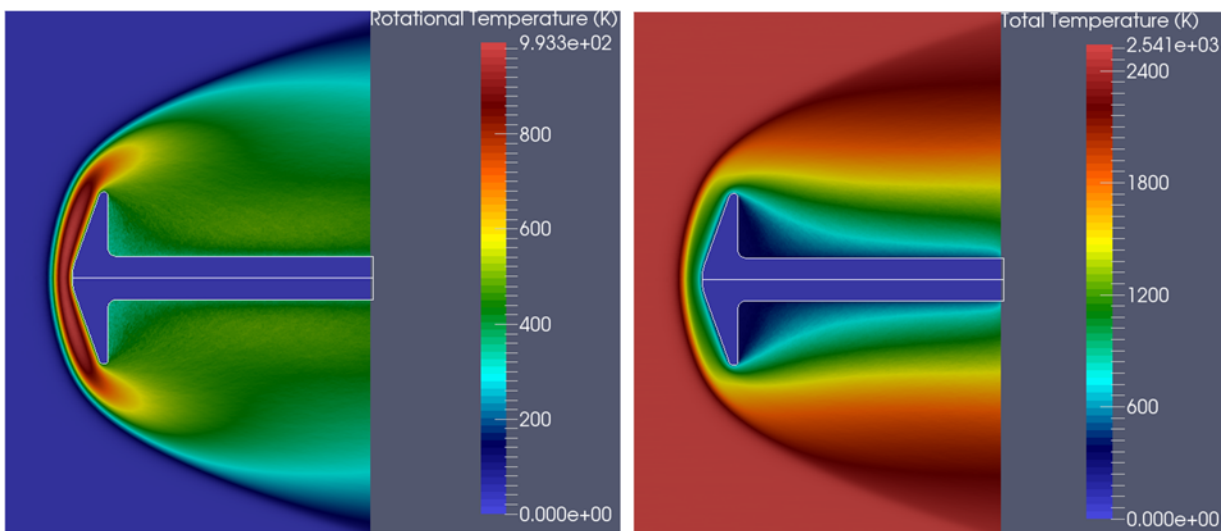

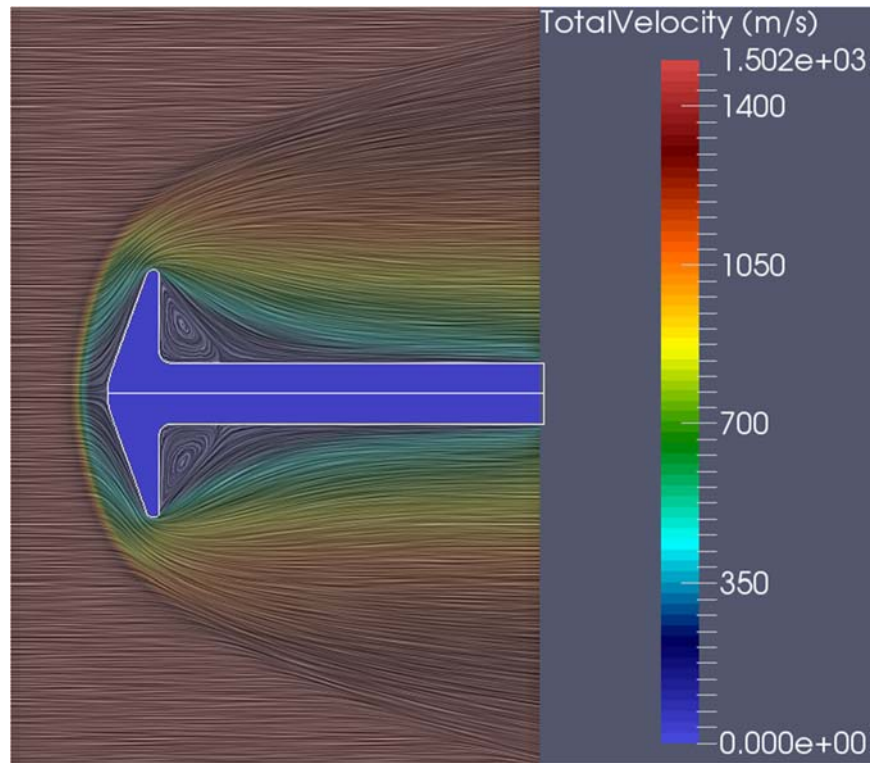Figure 3.22. (Left) Velocity along y-axis, (Right) Total temperature (case 2).

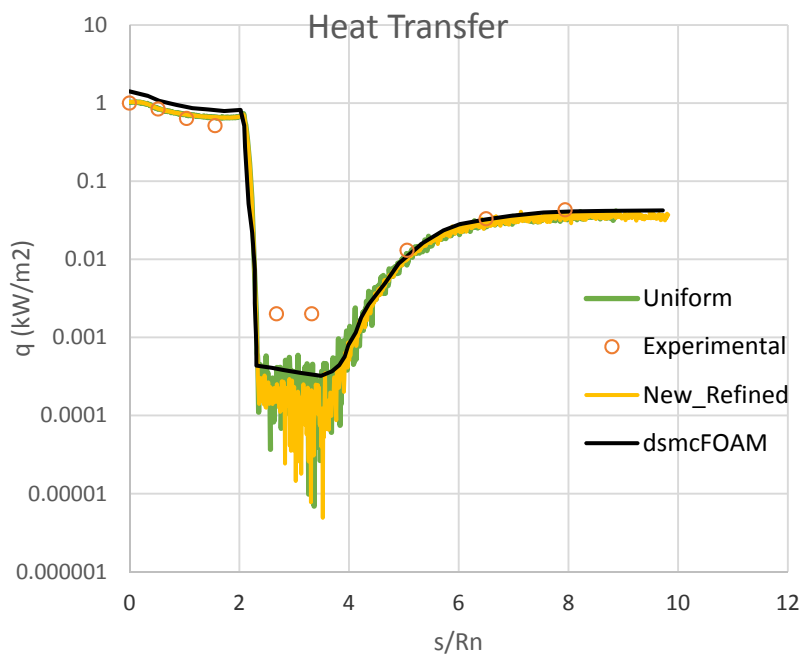Figure 3.23. Velocity magnitude streamlines (case 2).

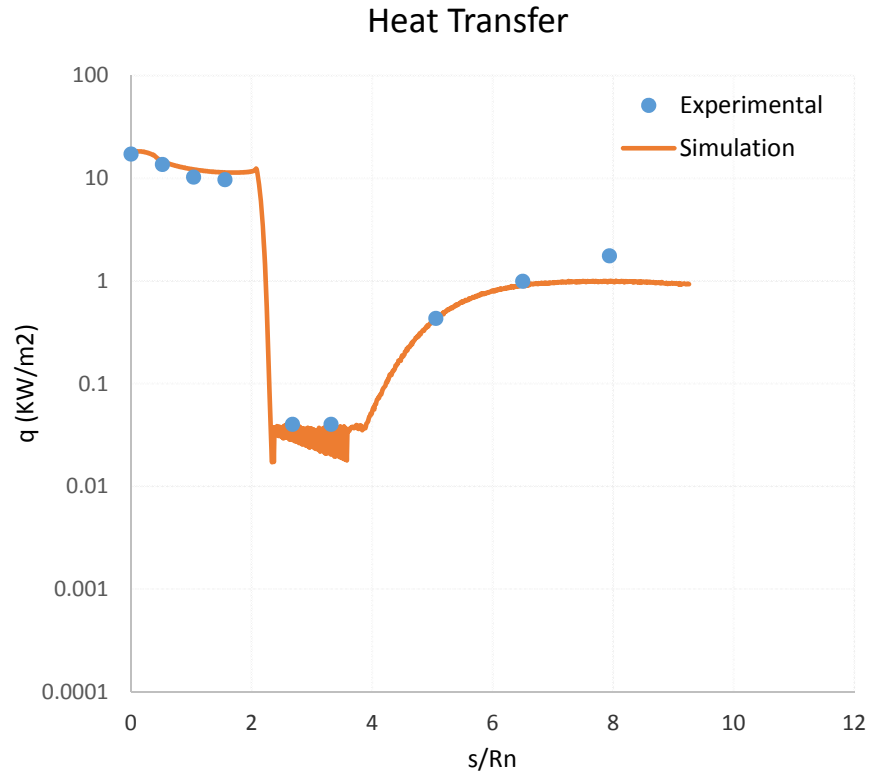Figure 3.24. Comparison of experimental and calculated heat transfer (case 1).

Figure 3.25. Comparison of experimental and calculated heat transfer (case 2).

3.4 Flow around a Flared Cylinder

3.4.1 Introduction

One of the most challenging problems of hypersonic computational aerodynamics is the accurate prediction of laminar flow separation in the near-continuum regime. Numerical solution of this problem for laminar flows is generally performed using the Navier-Stokes equations, and the effects for low Reynolds numbers are taken into account with the velocity slip and temperature jump boundary conditions. However for modelling the flow near the leading edge of a slender body, the use of the Navier-Stokes equations even with the conditions mentioned above is questionable. This is because the rarefaction effects are significant due to the merging of the shock wave and viscous layer and the flow physics are complicated when there is a flow separation. In order to improve the understanding of laminar separated flows, experimental and computational studies have been performed by the NATO Research Technology Organization for two different configurations, a hollow cylinder, a flare and a double cone. In this section only the flared cylinder case will be examined and at a later section the double cone. Several modelling of these configurations exist in literature using both the DSMC method and the Navier-Stokes approaches [42],[43],[44],[45],[46], . The main reason for this test case is to examine SPARTA applicability

to compute the near-continuum laminar flow with separation over a hollow cylinder with flare. A special attention has been given to the cell size around the flare and a comparison is given between a uniform grid and a refined grid around the flare.

3.4.2 Description of the hollow cylinder simulation

The flow conditions used in this simulation are the ones described in Ref. [15] for the Run 11. The conditions are summarized in Table 3.7. As far as grid is concerned in this case a 2-Level Cartesian grid with 957 by 440 cells in the x-axis and y-axis respectively was used with the refinement area starting at about 8cm after the leading edge and ending in the end of the flare. At the refined are each Level-1 cell is divided in 10 by 10 Level-2 cells. Before that a second uniform grid of 1000 by 1800 cells was considered with two different number of particles 2 million and 10 million. In the end the first grid was selected as it could capture adequately the flow characteristics in this area and the particles number reached a value of 17 million. The computational domain for this study was from -0.001m to 0.22m in the x-axis and from 0m to 0.12m in the y-axis. The hollow cylinder geometry is shown in Figure 3.26 and it comprises of a sharp leading edge with a 10-degree bevel aligned parallel to the incoming flow. The compression flare is at an angle of 30-degrees with the cylinder.

Condition	Flow Velocity (m/s)	Number Density, m⁻³	Flow temperature (K)	Gas	Surface Temperature (K)
LENS Run 11	2484	1.187×10^{22}	95.6	N_2	297.2

Table 3.8. Hollow flared cylinder flow conditions.
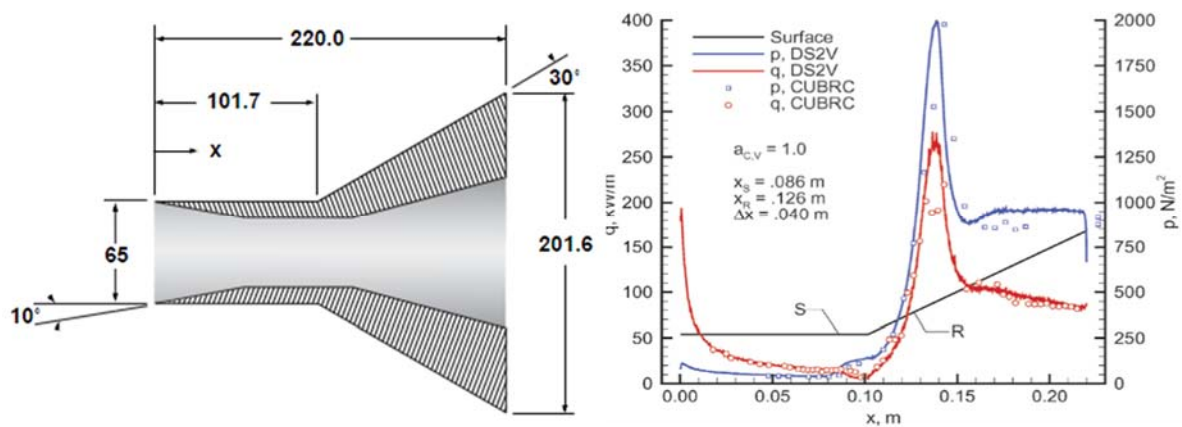
Figure 3.26.(Left) Hollow cylinder geometry (units in millimeters) [15], (Right) DS2V computed results [15].

48

Time-step	$2.0 \times 10^{-8} sec$
Particle weight	$4.4 \times 10^{18}\ real\ per\ simulated\ particles$
Transient period	$246000\ steps$
Sampling period	$12000\ steps$
Interval Sample data	2

Table 3.9. Hollow cylinder simulation parameters.

3.4.3 Results

The modelling of flows with separation in the near-continuum regime is a challenge for the DSMC method. On the results discussed below the calculations of using two different grids are shown, the uniform grid was tested with 2 million and 10 million particles, whereas the refined grid had 17 million particles. The pressure along the surface is shown in Figure 3.35 for all the examined cases. For the pressure calculation there is no impact of the grid on the cylinder upstream of the separation region and on the flare downstream of the shock interaction region. The most obvious difference is in the heating rate calculation in which the uniform grid produces unphysical results in the shock interaction region. By observing the temperature contours we can clearly see that the vibrational temperature has to be taken into account during the simulation as the temperature values yield for nonequilibrium thermal effects. In all calculations in this case the surfaces are assumed to have full thermal accommodation for the vibrational energy.

On the velocity contours plot we can see that there is a discontinuity of the flow below the cylinder's flat edge which leads to the formation of a barrel shock on the inside of the cylinder. As shown a Mach disk is present and there is also a separation region on the cylinder's internal surface. In Figures 3.35 and 3.36 there is a comparison between the simulation results and the available experimental data. There is a good agreement observed between the DSMC (refined grid) and the experimental results regarding the pressure and heating rate along the surface. In this case the DSMC applicability conditions were satisfied, enabling us to obtain the results that are in good agreement with the experimental data, and thus prove the applicability of the DSMC method to model this flow.

Moreover in this test case the results obtained are not only compared with the experimental ones but also with the results obtained from Moss and Bird using the DS2V solver [15]. The results of DS2V are shown in Figure 3.26 and were extracted from [15], using a graph data extractor. In DS2V the user has no authority over the grid as it is made exclusively by the code. That is one of the key features of DS2V in order to allow for less experienced users to be able to conduct DSMC simulations. Both codes underpredict in the cylinder's flared region in where DS2V seems to underpredict less than SPARTA. However in the pressure calculation SPARTA's results are more accurate.
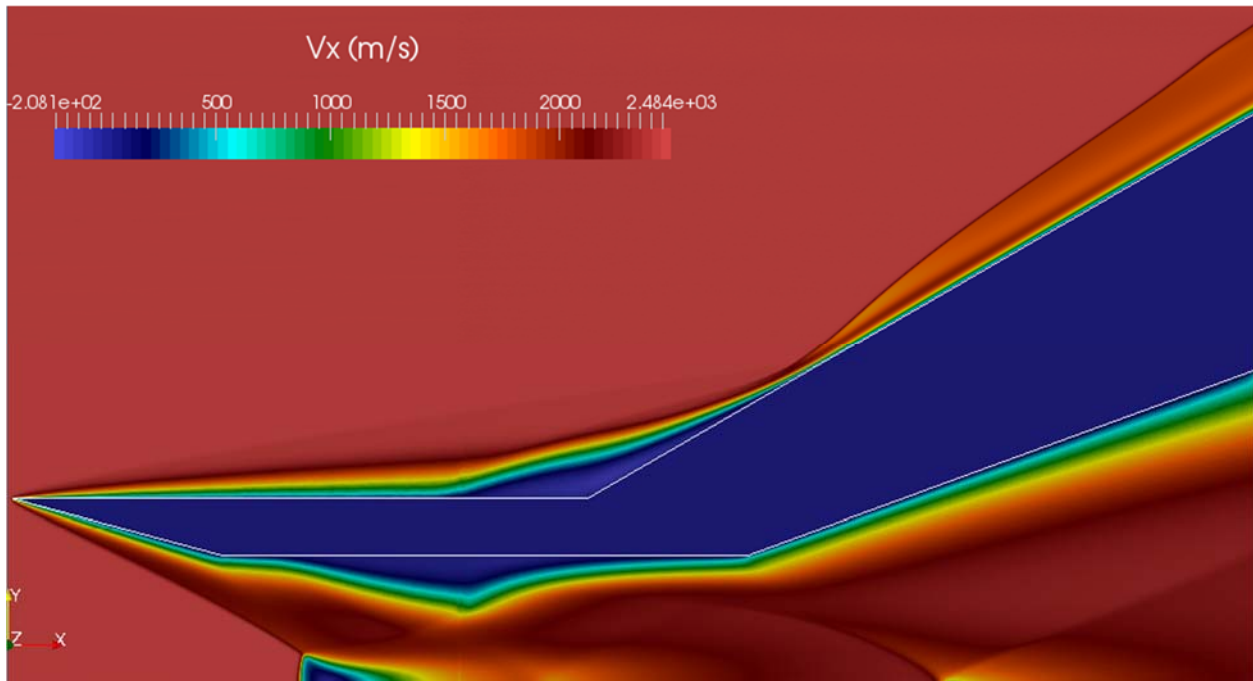
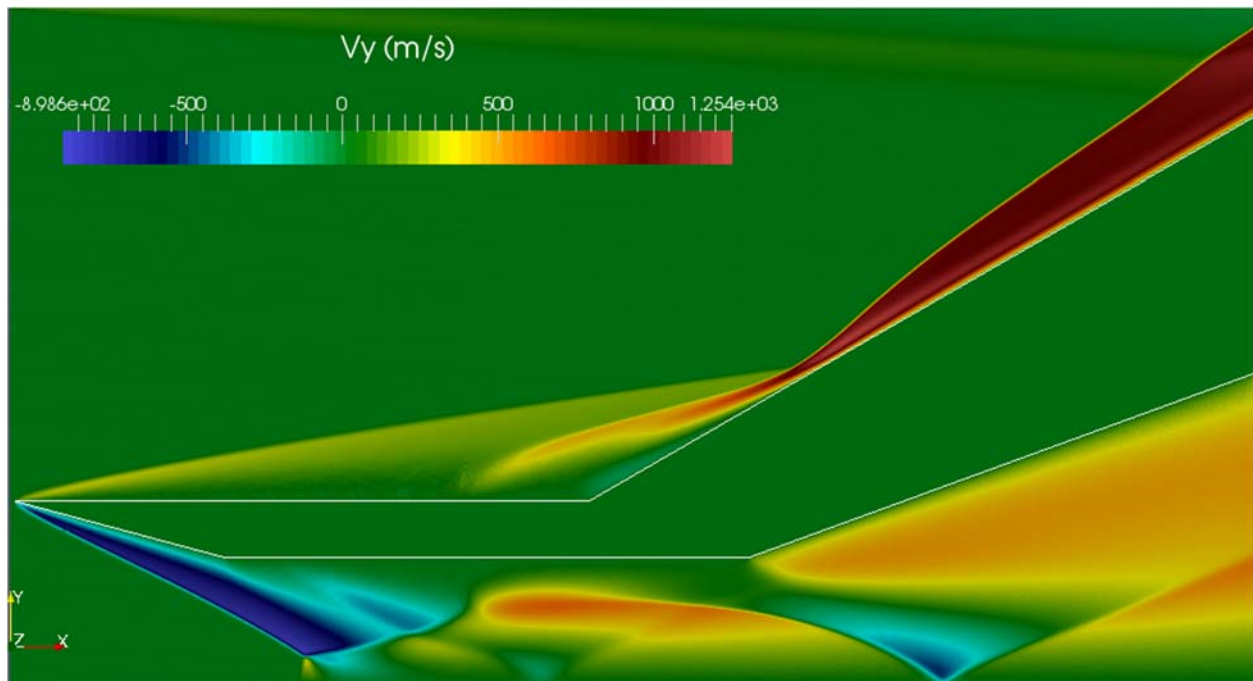Figure 3.27. Velocity along x-axis.

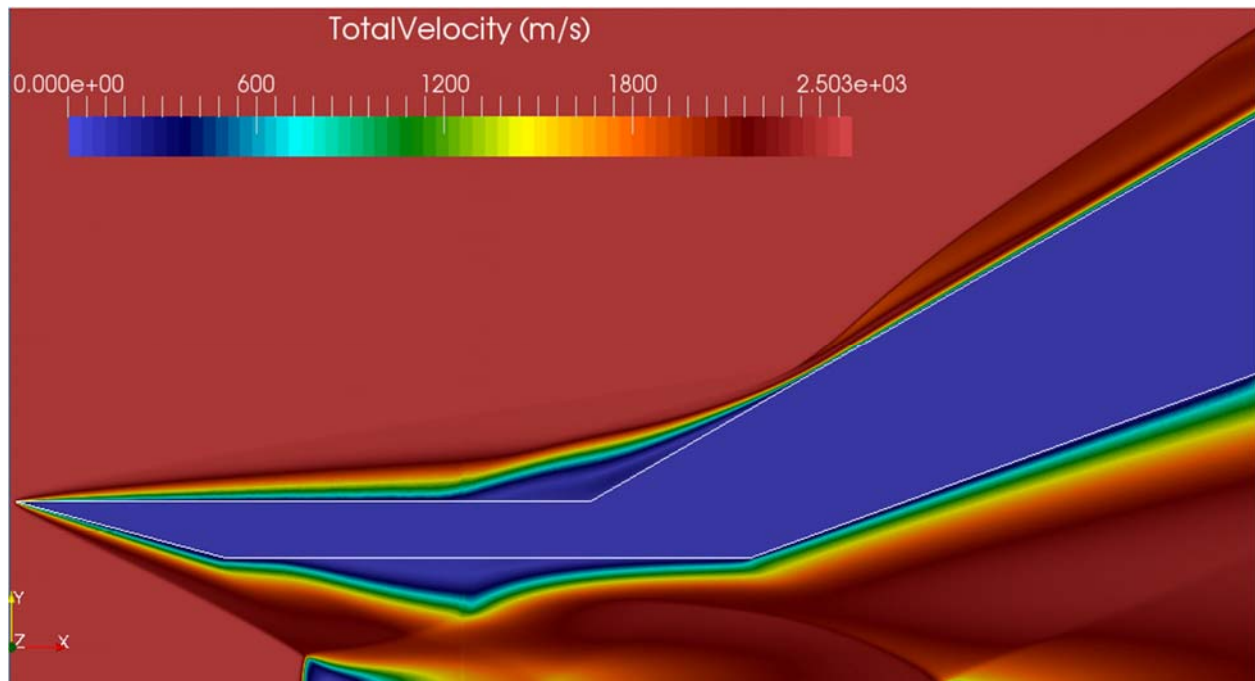Figure 3.28. Velocity along y-axis.
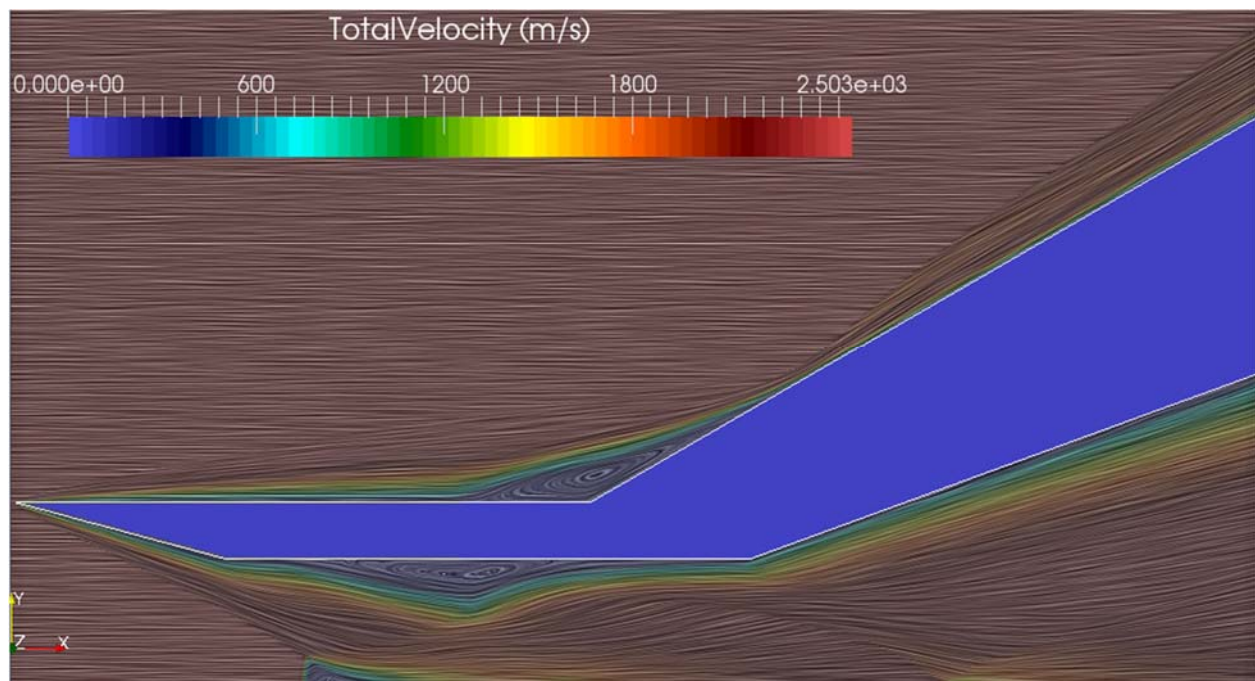
Figure 3.29. Velocity magnitude.

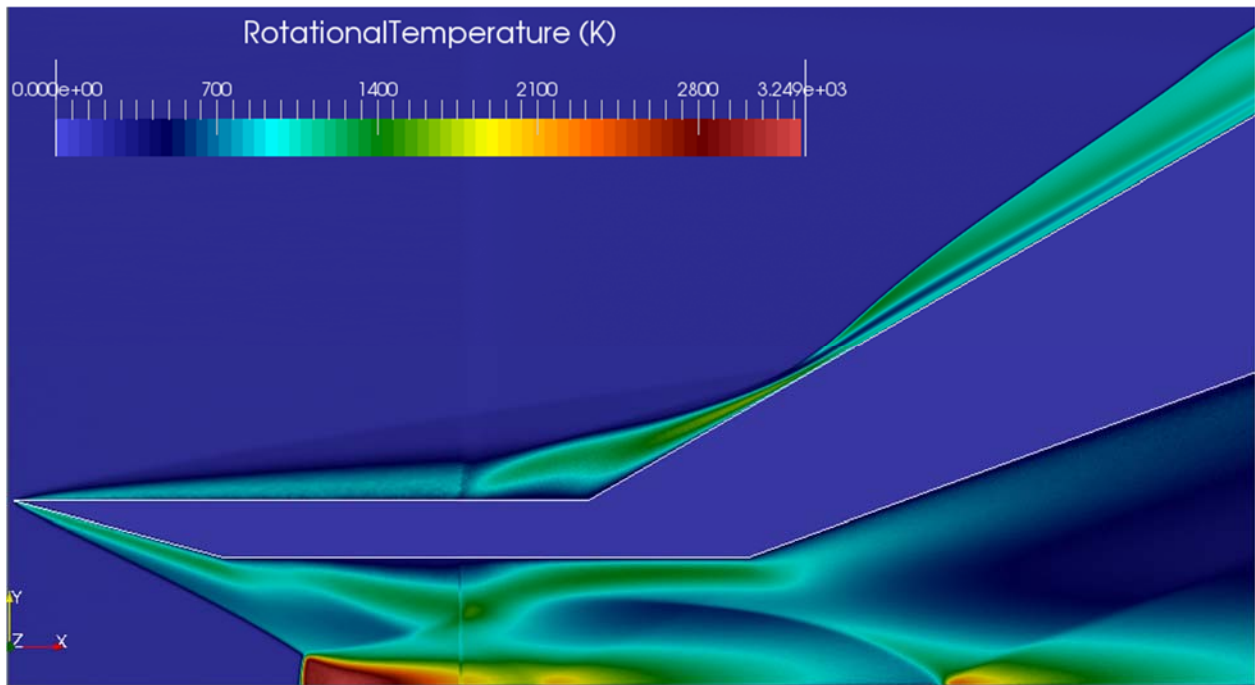Figure 3.30. Velocity magnitude flowlines.
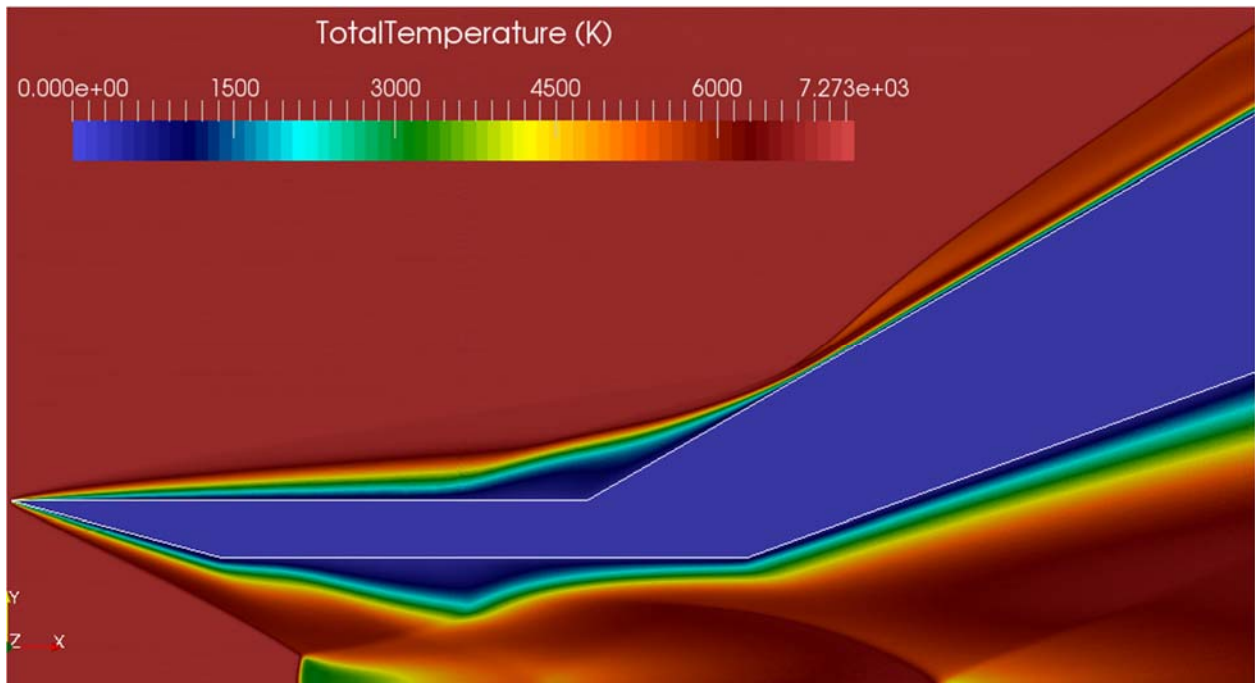
Figure 3.31. Rotational temperature.

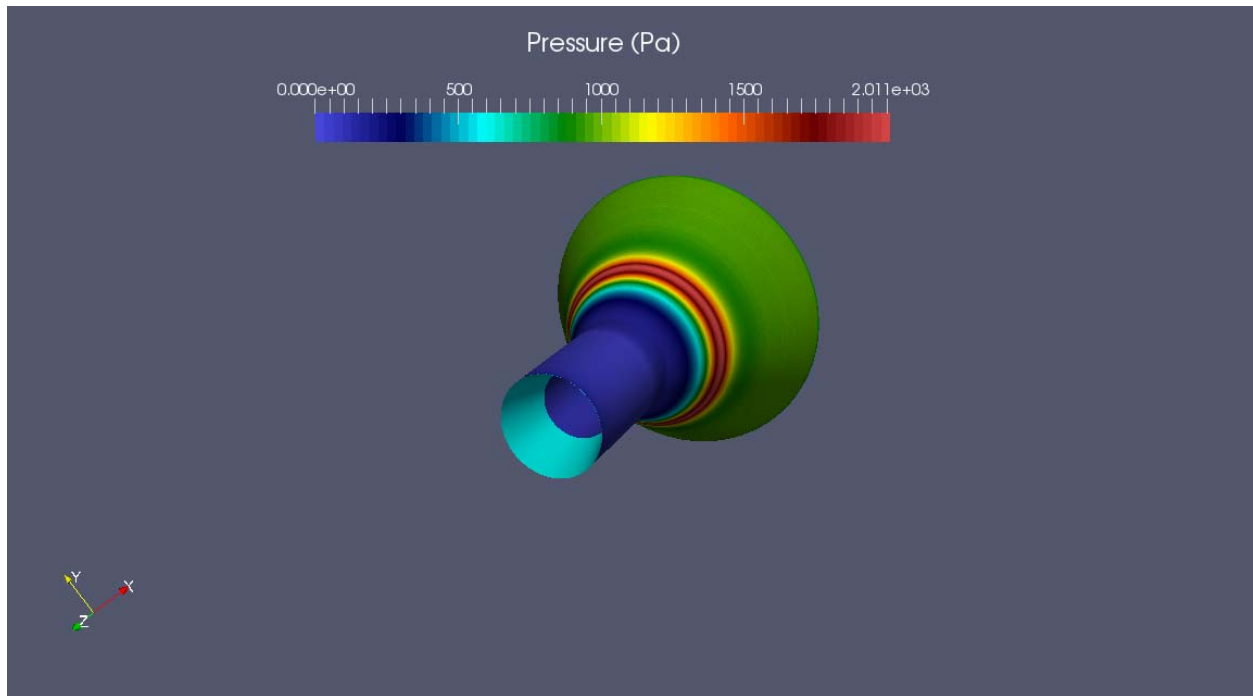Figure 3.32. Total temperature.

Figure 3.33. Pressure distribution along the surface.
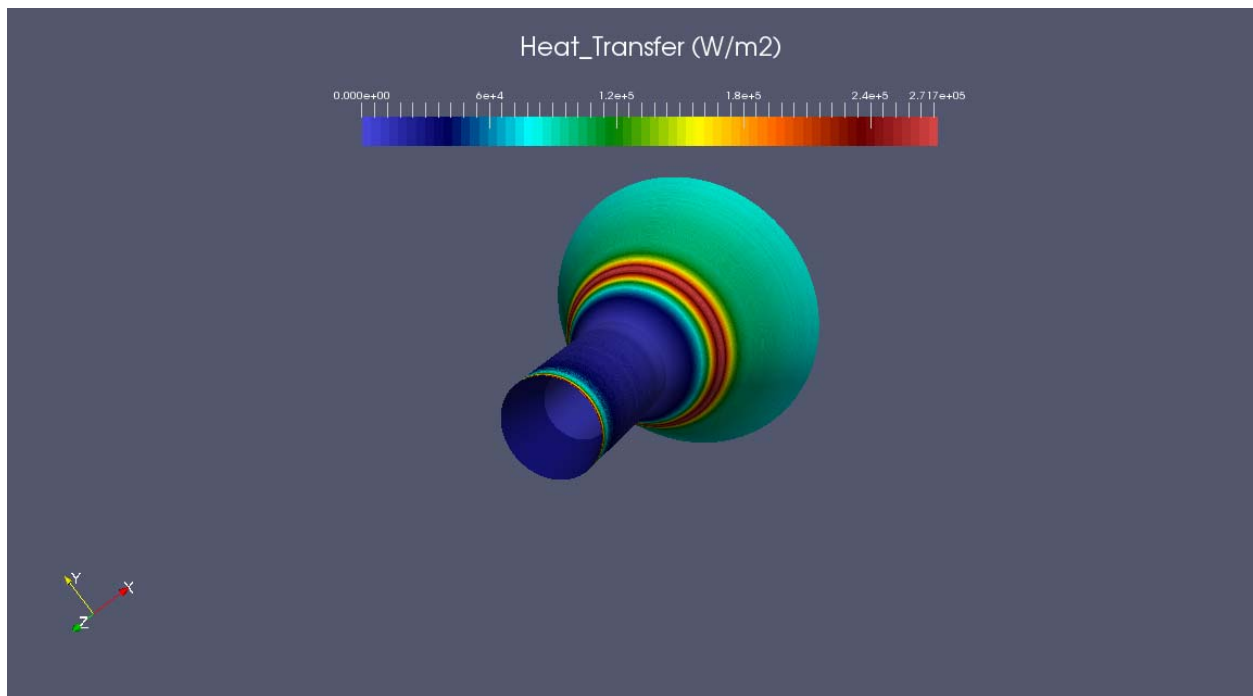

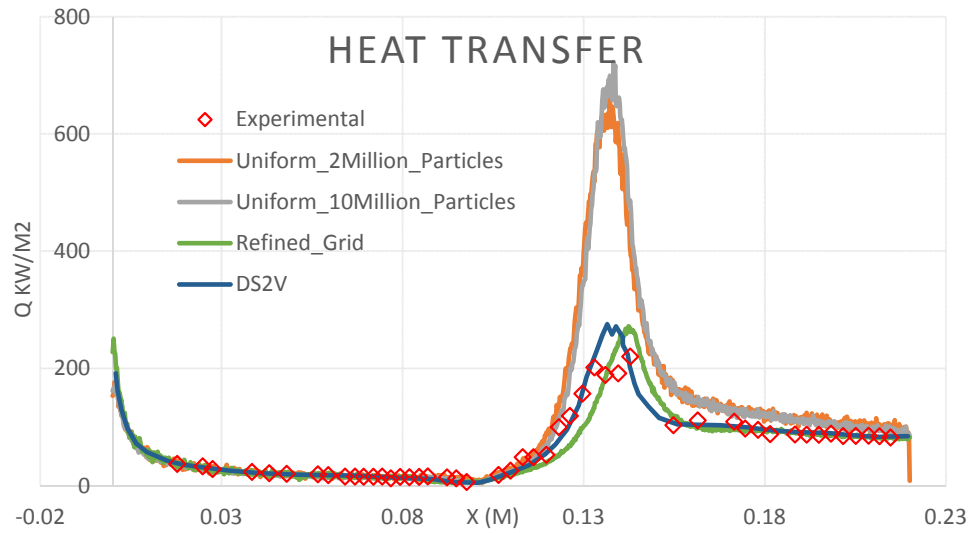Figure 3.34. Heat transfer along the surface.

Figure 3.35. Comparison of calculated and experimental heat transfer along the surface.
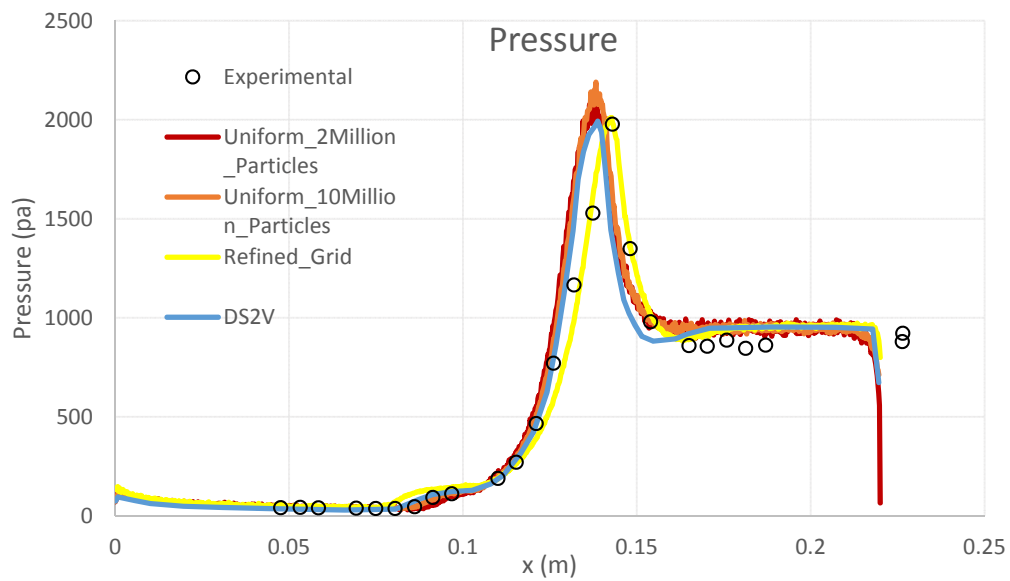

Figure 3.35. Comparison of calculated and experimental pressure along the surface.

3.5 Flow around a Biconic

3.5.1 Introduction

In this case the flow around a 25/55 degrees biconic geometry is examined. This geometry along with the flared cylinder geometry examined above are the two basic axisymmetric configurations proposed by the NATO Research Technology Organization in collaboration with the Working Group 10 [47],[48]. This particular test case was chosen due to the complex interactions resulting from hypersonic flow around this configuration. Various attempts have been made in the past using both CFD and DSMC methods for the simulation of several CUBRC experiments [49],[50],[51]. Judging from the simulation results from CFD and DSMC several significant findings have identified. One is that grid resolved DSMC solutions for the CUBRC biconic test conditions are not practical [46], and consequently the coarse grid solutions doesn't predict the correct details of the separation area. A second finding is that DSMC and CFD results for the heating rates upstream of the separation area can differ as much as 33% as discussed in Ref. [52] for laminar flow around either sharp [52] or blunted [53] cones at zero degrees angle.

The geometry of this test case comprises of two cones, one with a half angle of 25 degrees and a second one with a half angle of 55 degrees. The geometry is shown in Figure 3.36. This geometry produces strong shock interactions because the attached shock from the first cone interacts with the detached shock bow shock of the second cone. Moreover, the outer shocks are modified by separation and reattachment shocks.
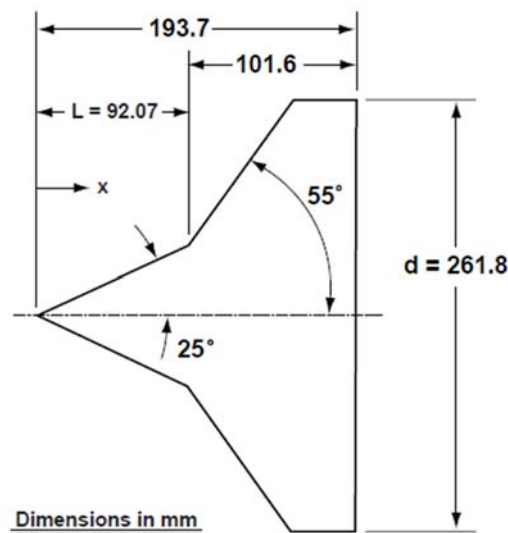

Figure 3.36. Double cone geometry [15].

3.5.2 Description of the 25/55 degree biconic simulation

Due to complex shock interactions developed during the simulation of this case in order to capture accurately the physical properties of the flow care must be given to the grid generation. The flow conditions are described in Table 3.11. Regarding the grid generation in this case a 2-Level grid was generated. The first level comprises of 870 by 870 cells in the x and y axis respectively, whereas the second level starts at about 5 cm after the biconic's leading edge and ends up at the end of the biconic. The dimensions of the flowfield domain are, 0.2m along the x-axis and 0.5m along the y-axis. In order to capture adequately the flow characteristics a number of 35 million particles was used. The computational domain for this test case is from -0.02m to 0.2m for the x-axis and from 0m to 0.2m for the y-axis. There are 2 different models for this case one with a blunt nose and an another one with a sharp edge [52], [53] but only the one with the sharp edge was considered for this case.

Condition	Flow Velocity (m/s)	Number Density, m^{-3}	Flow temperature (K)	Gas	Surface Temperature (K)
CUBRC Run 7	2072.6	3.78×10^{21}	42.61	N$_2$	297.2

Table 3.11. Biconic case flow conditions.

Time-step	$\mathbf{4.0 \times 10^{-8} sec}$
Particle weight	$\mathbf{3.0 \times 10^{18}\ real\ per\ simulated\ particles}$
Transient period	$\mathbf{250000\ steps}$
Sampling period	$\mathbf{27000\ steps}$
Interval Sample data	**2**

Table 3.12. Biconic case simulation parameters.

3.5.3 Results

On the results discussed below the results from all three studied grids are shown. Furthermore as mentioned in Ref. [50] for this specific case the flow stabilizes on the order of a millisecond. Despite this fact we let the flow to advance for more than a millisecond in real time in order to eliminate the numerical artifacts that can be generated from the flow stabilization phase. In Figures 3.37 and 3.38 the surface results are shown. As it can be seen from the Figures the uniform grid produced a good result for the first half of the biconic but on the flared region produced an unphysical result. This is due to the very steep flow gradients in this region generated from the shocks interaction. The second grid produced a better result than the first one but the result around the flow reattachment region is unreal. The third grid produced a rather physical result but at the end of the flared region the result was not accurate, this evidences how steep the flow gradients are and that a refined grid is needed also for some part of the biconic horizontal area so that the transition from the steep gradients to the less steep ones is accomplished smoothly. In this case the vibrational temperature is not tracked and full thermal accommodation is assumed for the gas-surface interactions.

Furthermore it can be noted that in this test case due to the elevated free stream pressure the grid used is large. The mean free path is at about 0.23 millimeters so taking into account the flow domain dimensions the level-1 cells are about 0.22 millimeter(little less than a mean free path) and on the flared region where the density rises especially around the flow reattachment point as it can be seen from Figure 3.39 each refined cell is 0.022 millimeter. Moreover from Figure 3.39 we can see that in the shocks interaction area the density is more than 40 times bigger than the one of the freestream. In Figures 3.40a and 3.40b the velocity along x and y axis and total velocity is shown respectively. By observing Figure 3.41a although the streamlines are not shown (due to computer RAM limitation) a small counter rotating vortex at the separation area exists. Also from the velocity Figures we can evidence that the shock off the forward part of the separation intersects the bow shock created by the second cone. From this intersection there is a transmitted shock which reflects off the surface of the biconic.

In Figures 3.42b, 3.43 and 3.44 the surface properties of the biconic are shown. In Figure 3.42b the heat flux stagnation point, which location is at the leading edge of the first cone can be identified. Furthermore in Figure 3.43 we can see the area where the most particles exist is before the middle of the second cone and this fact evidences the shocks interaction area. Finally in Figure 3.45 a grid close-up is presented where we can see a part of the refinement area. As shown the refinement ends at some point of the flat area of the second cone. The exact location of the refinement area end point can be found from Figures 3.37 and 3.38 where there is an area of an unphysical rise of the surface properties. This rise evidences that the flow gradients are still very steep although we approach the end of the biconic surface. In this test case the results obtained from a 2-level Cartesian grid are compared with the results obtained from dsmcFoam by using an unstructured grid. As far as dsmcFoam results are concerned they were obtained from Ref. [9] by using a graph extractor.
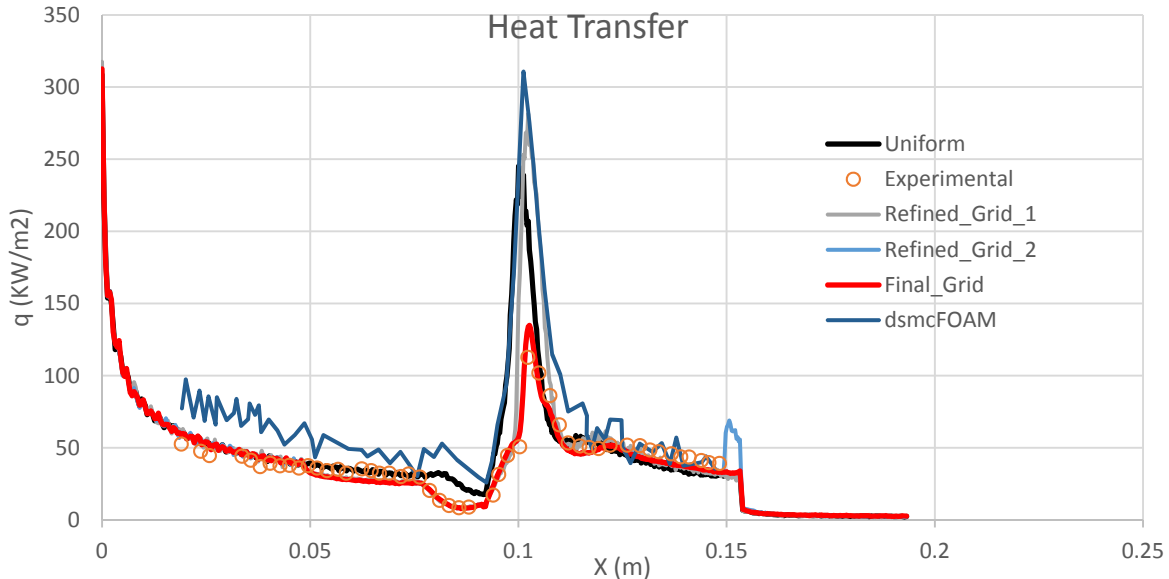

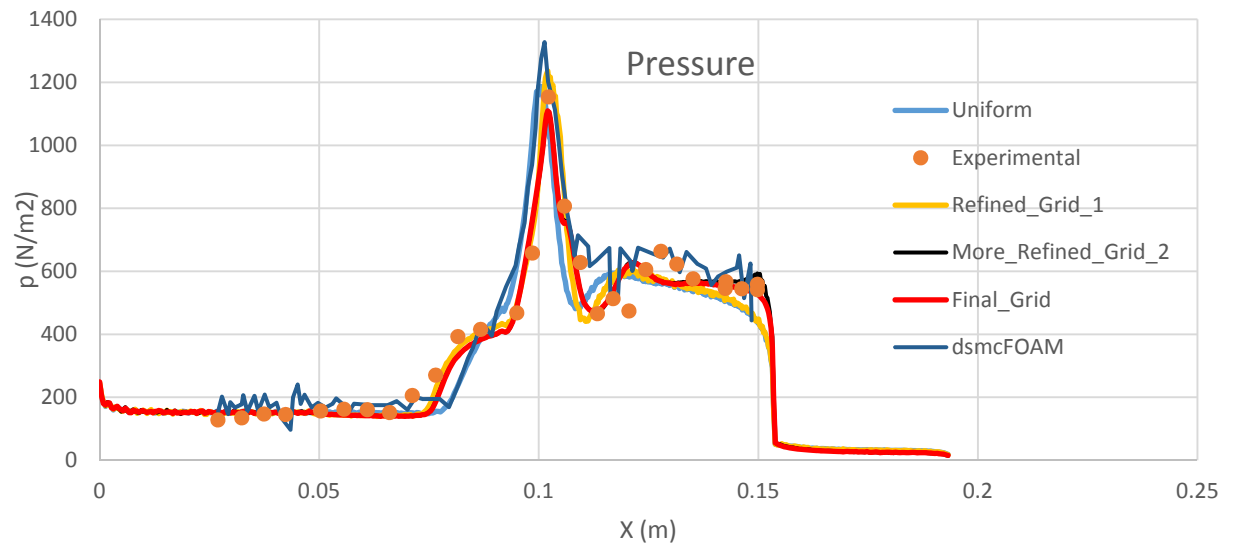*Figure 3.1. Heat transfer along the biconic surface*

Figure 3.2. Pressure distribution along the biconic surface.
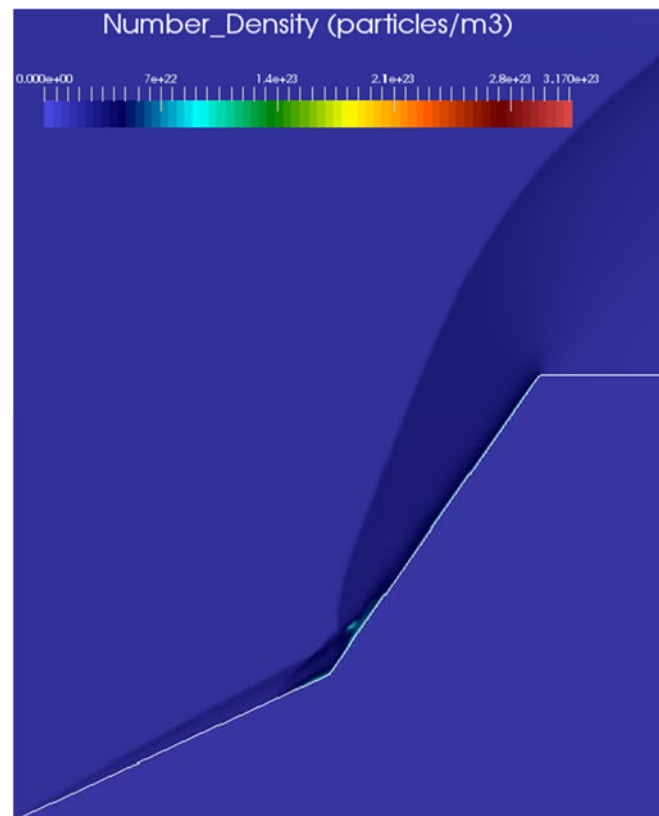
Figure 3.3. Number density plot.
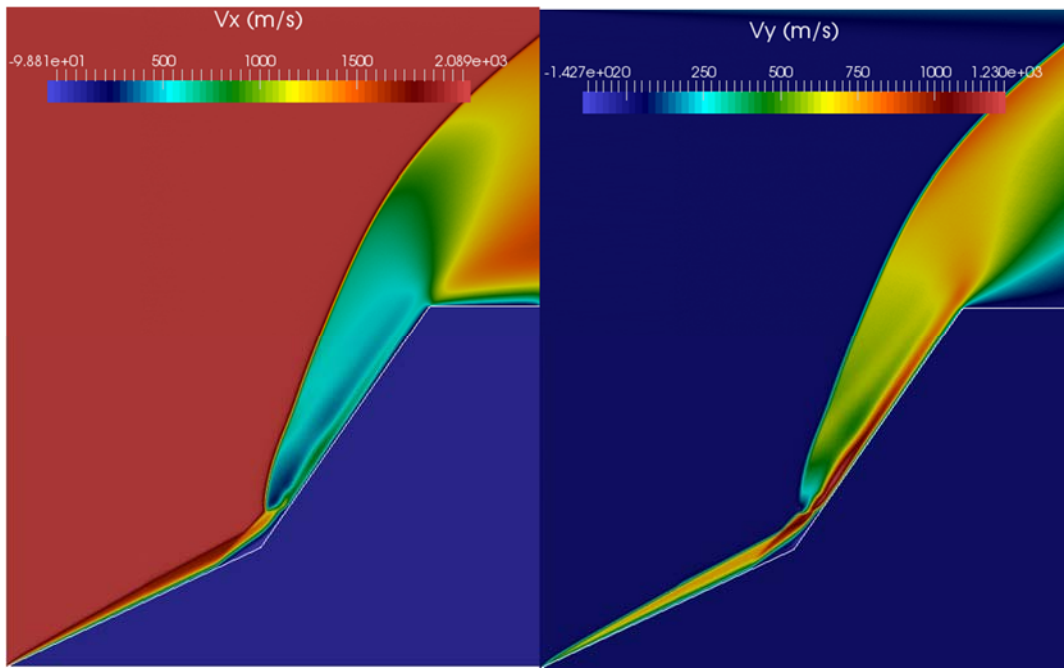
(a)   (b)

Figure 3.4. (a) Velocity plot across x-axis, (b) Velocity plot across y-axis.
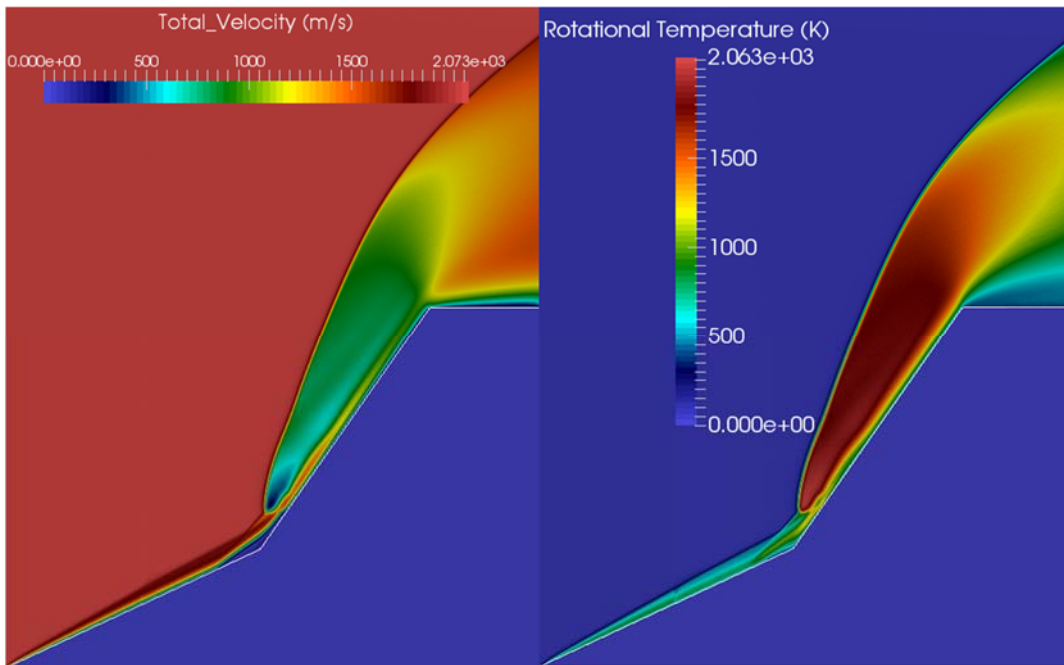
(a)   (b)

Figure 3.5. (a) Total velocity temperature plot, (b) Rotational temperature plot.
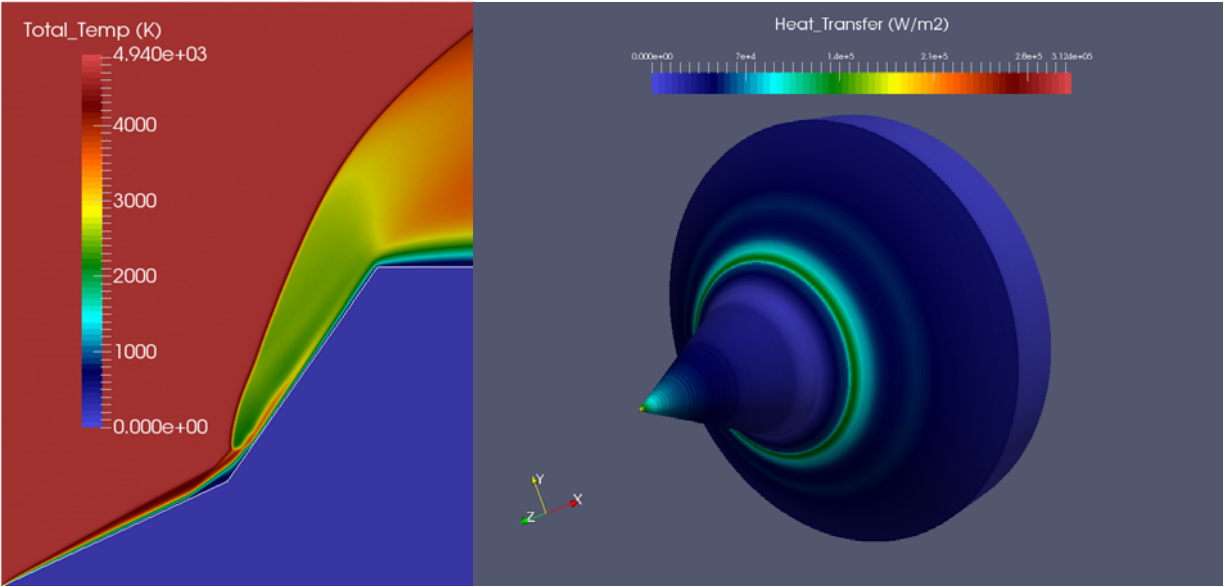
(a)   (b)

Figure 3.6. (a) Total temperature contours, (b) Surface heat transfer.
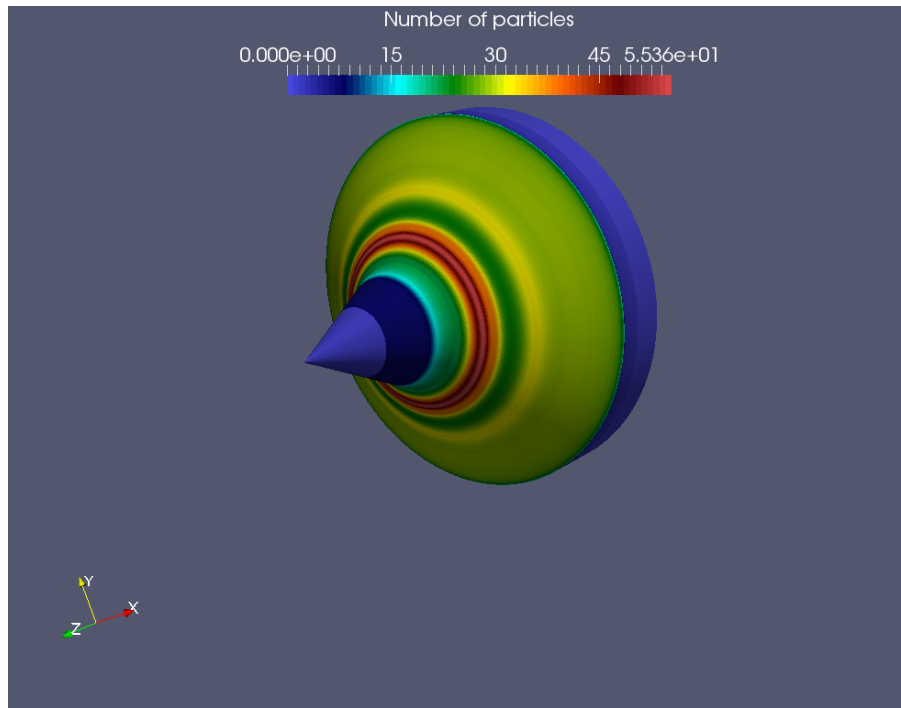
Figure 3.7. Number of particles that hit the surface.
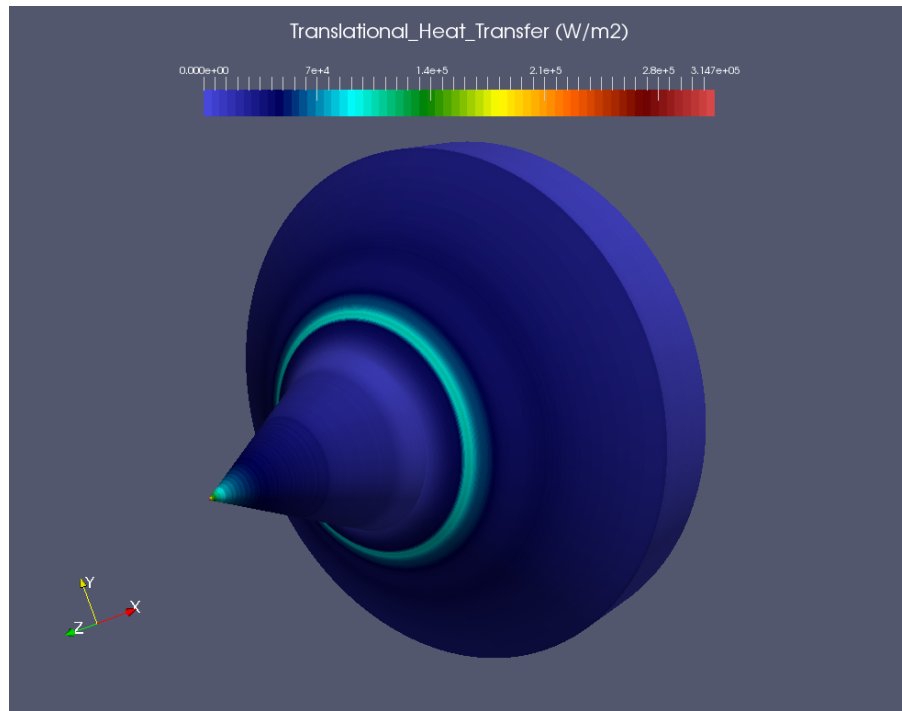
Figure 3.8. Translational heat transfer along the surface.

Figure 3.9. Flowfield grid close-up.

Conclusions

During the past few decades, there has been much research development regarding hypersonic vehicles applications. With the improvement of computational ability, more and more physical properties can be simulated by particle based methods such as the Direct Simulation Monte Carlo (DSMC) method. At its beginning the method was not widely accepted and it was used only for hypersonic rarefied gas dynamics problems such as calculating the heat and pressure distribution on the surfaces of re-en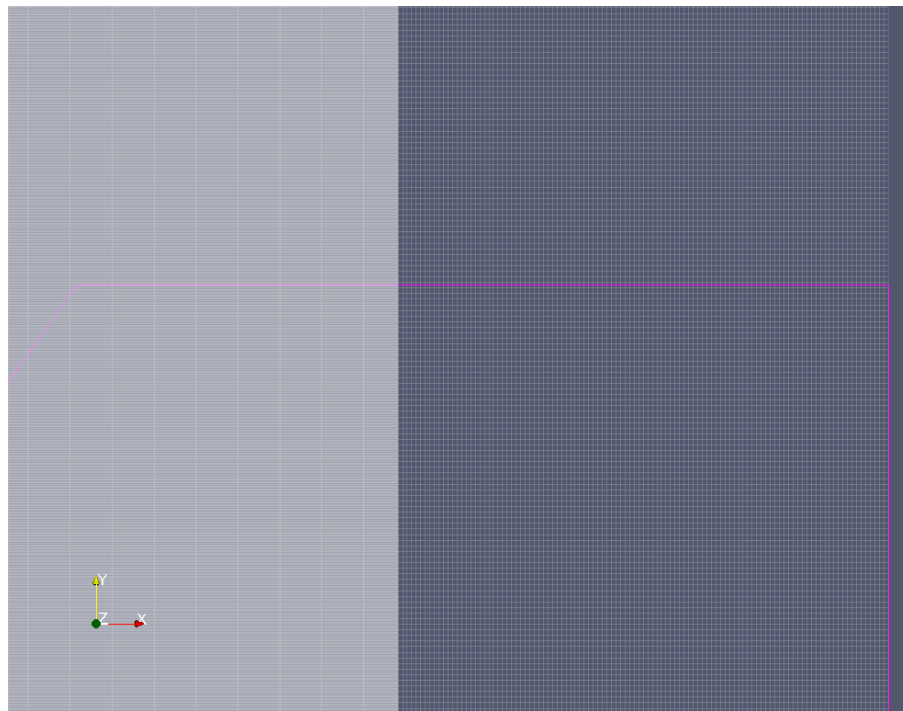try vehicles. Later the method was also extended to subsonic micro flows. In this work four different rarefied hypersonic flow cases have been examined. In all cases there is a very good agreement between the computed and the experimental results with the grids described for each case. Moreover it has been proved that by using a good quality grid SPARTA is capable to analyze accurately rarefied hypersonic flows. It has to be noted that the flows for the flared cylinder case and the biconic case have been analyzed with a small number of particles. Despite this fact due to the grid used the results are very accurate. In literature usually for this cases a very large number of particles is used for example in Ref. [47] Gimelshein et al. use 40 to 80 million particles in order to examine accurately the shocks specifications but the grids used are smaller than the ones used in SPARTA and there is no information about the refinement area.

As far as the flat plate simulation is concerned it will be worth for investigation the SPARTA scale up in more than 32 processors and compared with DAC scale up. This comparison has not been made in this work because not exact information has been found yet, either the exact case geometry was not defined accurately or the number of processors was not mentioned. Despite this fact SPARTA results are better than DAC in the heat transfer on the upper surface of the plate. Otherwise the results from both codes are in very good agreement except in the heat calculation where SPARTA seems to perform better than DAC. As far as the flared cylinder and the biconic cases are concerned it would be worthy to examine the results produced by SPARTA with the grids used in this work, but with a higher number of particles. For the simulations performed in this work the uniform grid produced a good result in the front and the back area of the cylinder and it fails to produce a physical in the shocks interaction area. This fact happens due to the very steep flow gradients in this area which the uniform grid cannot capture. The refined grid captures very well the gradients in this area in comparison with the uniform grid.

In the 70-degree blunt cone simulation the computed results were also in very good agreement with the experimental results. In this case a refined grid was used around the blunt cone only since this was the most important area examined. In the most rarefied case from the two examined the vortexes at the back of the cone are not very well resolved. This is not a grid issue but it is related with the rarefaction of the gas used. On the second test case for the blunt cone geometry where the gas is denser than in the first case we can clearly evidence the two vortexes in the back area of the cone. As far as the computed and the experimental results are concerned the agreement is excellent in the forecone area. In the back of the cone there is a slight difference between the computed and the experimental results. According to Ref. [13] this difference is explained by the fact that due to the gas rarefaction in this area the sensors used in the experiment could not resolve the flow data very well around this area. In the future a new simulation for the flared cylinder case is going to be released but with 40 million particles and using the ONERA R5Ch flared cylinder geometry from Ref. [55].

In the last case examined in this work the flow effects were complex and very challenging to compute. The biconic geometry produces very strong shock interactions due to the angle between the first and the

second cone. In this case despite the effort the DSMC assumptions of each cell dimension to be the one third of the flow mean free path and each particle to cross one cell in three timesteps could be full filled. Due to the strong shock interactions there are a few areas of very high density which is very challenging for the DSMC method to capture. Although the results obtained are in good agreement with the experimental results this case acquired much more time to simulate than the other three examined. Although not examined in the present work another run will be made in order to examine the case sensitivity in the particles number. Moreover one more effort will be made in order to try and fulfill the DSMC assumptions as mentioned above, although we still cannot be sure about the computational cost and the impact that this will have to the computed result.

This work also reveals that multi-level Cartesian grids can produce results that are of almost equal quality to results produced by conforming grids of DS2V, for rarefied hypersonic flows. Moreover because of their simplicity it is relatively easy to implement grid data communication techniques and grid decomposition algorithms. Due to their simplicity they are memory efficient, this fact allows us to solve big problems in systems with not so much memory. But despite their advantages they do have a major disadvantage, in order to get accurate results in the surfaces of the grid, advanced cut-cell algorithms are required.

In this work SPARTA performance was tested for 2d and 2d-axisymmetric flows by using some of the most demanding cases found in literature. In the near future a serious concern will be given in 3d simulations for real life applications. One application in which the code should be tested is the performance of various space and CRV (Crew Return Vehicle) vehicles in atmosphere reentry conditions were very high temperatures and plasma occur. Moreover reentries in different atmospheres than earths will also be tested, in order to study the flow effects in low density plasmas of other planets. As a concluding remark must noted that the code performance and results will also be measured in a some special flow categories such as microflows/nanoflows and under expanded free jets, it would be quite interesting to evidence SPARTA results in such a small scale.

Contributions

During this work the following contributions were made in order to resolve some bugs of the code and increase code's redundancy.

13 Jan 2015

Fixed an occasional bug with axisymmetric moves that could cause a particle to end up in the wrong grid cell when being communicated to a new processor. This is with the global gridcut command set to a positive finite value.

Thanks to Angelos Klothakis for sending a test geometry that had the problem.

17 Feb 2015

Fixed bug in restart files not including the global weight cell command setting if it was enabled, which was added for axisymmetric geometries.

Thanks to Angelos Klothakis for sending a script that triggered this issue.

5 Mar 2015

Fixed a memory issue when performing reactions on a problem where collisions are performed for multiple species groups within each grid cell.

Also fixed a logic bug with clipping multiple successive surfaces, read in by the read_surf command.

Thanks to Arnaud Borner (NASA Ames) and Aggelos Klothakis for sending test problem that triggered the issues

References

[1]   G. A. Bird, *Molecular Gas Dynamics and the Direct Simulation of Gas Flows*, 2nd edition. Oxford : New York: Oxford University Press, 1994.

[2]   M. A. Gallis, J. R. Torczynski, S. J. Plimpton, D. J. Rader, and T. Koehler, "Direct simulation Monte Carlo: The quest for speed," in *AIP Conference Proceedings*, 2014, vol. 1628, pp. 27–36.

[3]   G. J. LeBeau, "A parallel implementation of the direct simulation Monte Carlo method," *Comput. Methods Appl. Mech. Eng.*, vol. 174, no. 3, pp. 319–337, 1999.

[4]   M. I. G. Markelovf and S. F. Gimelshein, "Statistical simulation of reactive rarefied flows: numerical approach and applications," 1998.

[5]   S. Dietrich and I. D. Boyd, "Scalar and parallel optimized implementation of the direct simulation Monte Carlo method," *J. Comput. Phys.*, vol. 126, no. 2, pp. 328–342, 1996.

[6]   T. J. Bartel, S. Plimpton, and M. A. Gallis, "Icarus: A 2-D Direct Simulation Monte Carlo (DSMC) Code for Multi-Processor Computers," *User's Man. Version*, vol. 10, 2001.

[7]   D. Gao and T. E. Schwartzentruber, "Optimizations and OpenMP implementation for the direct simulation Monte Carlo method," *Comput. Fluids*, vol. 42, no. 1, pp. 73–81, 2011.

[8]   T. J. Scanlon, E. Roohi, C. White, M. Darbandi, and J. M. Reese, "An open source, parallel DSMC code for rarefied gas flows in arbitrary geometries," *Comput. Fluids*, vol. 39, no. 10, pp. 2078–2089, 2010.

[9]   A. O. Ahmad, T. J. Scanlon, and J. M. Reese, "Capturing Shock Waves Using an Open-Source, Direct Simulation Monte Carlo (DSMC) Code," 2011.

[10]   J. N. Moss, G. J. LeBeau, and C. E. Glass, "Hypersonic Shock Interactions About a 25 deg/65 deg Sharp Double Cone," Aug. 2002.

[11]   I. D. Boyd, "Direct Simulation Monte Carlo for Atmospheric Entry. 2. Code Development and Application Results," DTIC Document, 2009.

[12]   J. Allegre, M. Raffin, A. Chpoun, and L. Gottesdiener, "Rarefied hypersonic flow over a flat plate with truncated leading edge," *Prog. Astronaut. Aeronaut.*, vol. 160, pp. 285–285, 1994.

[13]   All-ccedil J., gre, D. Bisch, and J. C. Lengrand, "Experimental rarefied heat transfer at hypersonic conditions over 70-degree blunted cone," *J. Spacecr. Rockets*, vol. 34, no. 6, pp. 724–728, 1997.

[14]   All-ccedil J., gre, D. Bisch, and J. C. Lengrand, "Experimental Rarefied Density Flowfields at Hypersonic Conditions over 70-Degree Blunted Cone," *J. Spacecr. Rockets*, vol. 34, no. 6, pp. 714–718, Nov. 1997.

[15]   J. N. Moss and G. A. Bird, "Direct simulation Monte Carlo simulations of hypersonic flows with shock interactions," *AIAA J.*, vol. 43, no. 12, pp. 2565–2573, 2005.

[16]   J. N. Moss, "DSMC Simulation of Separated Flows About Flared Bodies at Hypersonic Conditions," presented at the European Congress on Computational Methods in Applied Sciences and Engineering, Barcelona, Spain, 2000.

[17]   G. A. Bird, "The DS2V/3V Program Suite for DSMC Calculations," in *AIP Conference Proceedings*, 2005, vol. 762, pp. 541–546.

[18]   M. Gallis, J. Torczynski, D. Rader, and G. Bird, "Accuracy and Convergence of a New DSMC Algorithm," 2008.

[19]   K. Koura and H. Matsumoto, "Variable soft sphere molecular model for air species," *Phys. Fluids Fluid Dyn. 1989-1993*, vol. 4, no. 5, pp. 1083–1085, May 1992.

[20]   G. A. Bird, "Recent advances and current challenges for DSMC," *Comput. Math. Appl.*, vol. 35, no. 1–2, pp. 1–14, Jan. 1998.

[21]   H. A. Hassan and D. B. Hash, "A generalized hard-sphere model for Monte Carlo simulation," *Phys. Fluids Fluid Dyn. 1989-1993*, vol. 5, no. 3, pp. 738–744, Mar. 1993.

[22] J. Fan, "A generalized soft-sphere model for Monte Carlo simulation," *Phys. Fluids 1994-Present*, vol. 14, no. 12, pp. 4399–4405, Dec. 2002.

[23] B. L. Haas, D. B. Hash, G. A. Bird, F. E. Lumpkin III, and H. A. Hassan, "Rates of thermal relaxation in direct simulation Monte Carlo methods," *Phys. Fluids 1994-Present*, vol. 6, no. 6, pp. 2191–2201, 1994.

[24] J. G. Parker, "Rotational and Vibrational Relaxation in Diatomic Gases," *Phys. Fluids*, vol. 2, no. 4, p. 449, 1959.

[25] D. B. Hash, H. A. Hassan, and J. N. Moss, "Direct simulation of diatomic gases using the generalized hard sphere model," *J. Thermophys. Heat Transf.*, vol. 8, no. 4, pp. 758–764, 1994.

[26] I. J. Wysong and D. C. Wadsworth, "Assessment of direct simulation Monte Carlo phenomenological rotational relaxation models," *Phys. Fluids 1994-Present*, vol. 10, no. 11, pp. 2983–2994, 1998.

[27] K. Koura, "A generalization for Parker rotational relaxation model based on variable soft sphere collision model," *Phys. Fluids 1994-Present*, vol. 8, no. 5, pp. 1336–1337, 1996.

[28] C. Shen, *Rarefied Gas Dynamics*. Berlin, Heidelberg: Springer Berlin Heidelberg, 2005.

[29] "Sparta User's Manual.pdf." .

[30] J. F. Padilla, "Comparison of DAC and MONACO DSMC Codes with Flat Plate Simulation," 2010.

[31] R. G. Wilmoth, G. J. LeBeau, and A. B. Carlson, "DSMC grid methodologies for computing low-density, hypersonic flows about reusable launch vehicles," *AIAA Pap.*, vol. 1812, 1996.

[32] F. E. Lumpkin III, P. C. Stuart, and G. J. LeBeau, "Enhanced analyses of plume impingement during Shuttle-Mir docking using a combined CFD and DSMC methodology," *AIAA Pap.*, vol. 1877, 1996.

[33] F. E. Lumpkin III, P. C. Stuart, and G. G. LeBeau, "The airlock depressurization plume anomaly on the STS-82 Hubble servicing mission," *AIAA Pap.*, vol. 462, 2000.

[34] D. S. Liechty, "Aeroheating analysis for the Mars Reconnaissance Orbiter with comparison to flight data," *J. Spacecr. Rockets*, vol. 44, no. 6, pp. 1226–1231, 2007.

[35] J. N. Moss, G. J. LeBeau, R. C. Blanchard, and J. M. Price, "Rarefaction effects on Galileo probe aerodynamics," 1996.

[36] C. E. Glass and T. J. Horvath, "Comparison of a 3-D CFD-DSMC Solution Methodology With a Wind Tunnel Experiment," 2002.

[37] "http://sparta.sandia.gov/pictures.html, 'Flow around Mir space station', Sandia National Laboratories." Oct-2014.

[38] "http://sparta.sandia.gov/pictures.html, 'Richtmyer/Meshkov mixing', Sandia National Laboratories." Oct-2014.

[39] J. Muylaert, A. Kumar, and C. Dujarric, *Hypersonic experimental and computational capability, improvement and validation*. North Atlantic Treaty organization, Advisory Group for Aerospace Research & Development, 1998.

[40] J. N. Moss, J. M. Price, V. K. Dogra, and D. B. Hash, "Comparison of DSMC and experimental results for hypersonic external flows," *AIAA Pap.*, vol. 2028, 1995.

[41] J. Allegre and D. Bisch, "Experimental study of a blunted cone at rarefied hypersonic conditions," *CNRS Meudon CNRS Rep. RC*, pp. 94–7, 1994.

[42] J. N. Moss, "DSMC computations for regions of shock/shock and shock/boundary layer interaction," *AIAA Pap.*, vol. 1027, p. 2001, 2001.

[43] I. D. Boyd and W.-L. Wang, "Monte Carlo computations of hypersonic interacting flows," *AIAA Pap.*, vol. 1029, p. 2001, 2001.

[44] P. A. Gnoffo and others, "CFD validation studies for hypersonic flow prediction," *AIAA Pap.*, vol. 1025, p. 2001, 2001.

[45] G. V. Candler, I. Nompelis, and M.-C. Druguet, "Navier-stokes predictions of hypersonic double-cone and cylinder-flare flow fields," *AIAA Pap.*, vol. 1024, p. 2001, 2001.

[46] S. F. Gimelshein, D. A. Levin, G. N. Markelov, A. N. Kudryavtsev, and M. S. Ivanov, "Statistical Simulation of Laminar Separation in Hypersonic Flows: Numerical Challenges," *AIAA Pap.*, vol. 736, p. 2002, 2002.

[47] D. Knight, "RTO WG 10 - Test cases for CFD validation of hypersonic flight," in *40th AIAA Aerospace Sciences Meeting & Exhibit*, American Institute of Aeronautics and Astronautics.

[48] S. Walker and J. D. Schmisseur, "CFD validation of shock-shock interaction flow fields," DTIC Document, 2006.

[49] G. V. Candler, I. Nompelis, M.-C. Druguet, M. S. Holden, T. P. Wadhams, I. D. Boyd, and W.-L. Wang, *CFD validation for hypersonic flight: hypersonic double-cone flow simulations*. Defense Technical Information Center, 2006.

[50] J. N. Moss, G. A. Bird, and G. N. Markelov, "DSMC simulations of hypersonic flows and comparison with experiments," DTIC Document, 2005.

[51] W.-L. Wang and I. D. Boyd, "Hybrid DSMC-CFD simulations of hypersonic flow over sharp and blunted bodies," *AIAA Pap.*, vol. 3644, p. 2003, 2003.

[52] J. N. Moss, *Hypersonic flows about a 25° sharp cone*. Citeseer, 2001.

[53] C. J. Roy, T. J. Bartel, M. A. Gallis, and J. L. Payne, "DSMC and Navier-Stokes predictions for hypersonic laminar interacting flows," *AIAA Pap.*, vol. 1030, p. 2001, 2001.